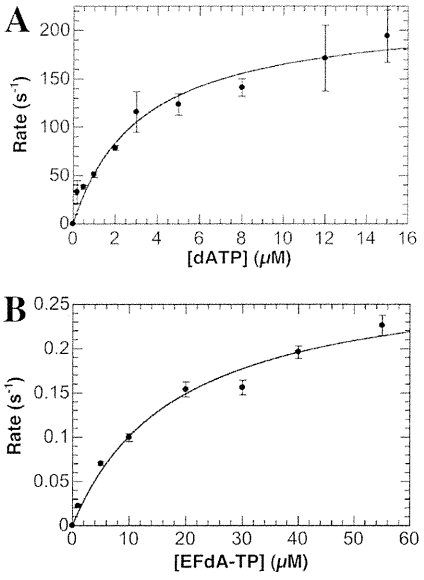

FIG 2 Concentration dependence of the observed rate of nucleotide incorporation by Pol γ. Each point in the plots represents the observed rate generated from fitting a time course with 10 different points using a double exponential equation (dATP) or a single exponential equation (EFdA-TP) (KaleidaGraph). The error bars in the plots represent the deviance from these exponential fits, and the standard errors associated with the determined rate constant values represent the deviance from the hyperbolic fits shown. (A) Observed rates of incorporation were plotted against dATP concentration and fit with a hyperbolic equation to generate a k_{pol} value of 220 ± 16 s^{-1} and a K_d value of 3.2 ± 0.7 μM. (B) Observed rates of incorporation were plotted against EFdA-TP concentration and fit with a hyperbolic equation to generate a k_{pol} value of 0.29 ± 0.02 s^{-1} and a K_d value of 18 ± 4 μM.

ing nucleotide, as described previously (7, 11). Wild-type (WT) Pol γ (exonuclease deficient) catalytic subunit (Pol γA) and accessory subunit were purified and reconstituted as described elsewhere (22, 23, 29). A KinTek Instruments RQF-3 rapid chemical quench was used to mix Pol γ holoenzyme and substrate, a 5′-radiolabeled DNA primer annealed to a DNA template (D21/D36 substrate) (Fig. 1B), with magnesium chloride and various concentrations of dATP or EFdA-triphosphate (EFdA-TP). The reaction was quenched with EDTA, and reaction mixtures were separated on a 20% polyacrylamide denaturing gel and analyzed by phosphorimaging (Bio-Rad Molecular Imager FX). Plots of product formation versus time were fit to single-exponential (EFdA-TP) or double-exponential (dATP) equations to generate k_{obs} (observed rate) values, which were plotted against nucleotide concentration and fit to a hyperbola to generate k_{pol} and K_d (KaleidaGraph; Synergy) (Fig. 2).

Pol γ incorporated EFdA-TP 760-fold more slowly and with 5.6-fold-lower affinity than the natural dATP substrate (Table 1). The efficiency of EFdA-TP incorporation (0.016 $\mu M^{-1}\ s^{-1}$) is well within the range of NRTIs on the market, showing 340- and 1.5-fold improvement over stavudine and didanosine, respectively (11). Although lower efficiencies are seen with tenofovir (3.2-fold) and AZT (16-fold) (11), it is important to remember that EFdA in the steady state showed 440-fold- and 66,000-fold-higher potency than AZT and tenofovir, respectively (24). Importantly, in contrast to RT, which shows a 2-fold selectivity for EFdA-TP over dATP in steady-state studies (24), Pol γ shows a 4,300-fold preference for the natural dATP substrate over EFdA-TP (Table 1), and this coupled

TABLE 1 Pre-steady-state rate constants for dNTP incorporation by Pol γ[a]

Nucleotide	k_{pol} (s^{-1})	K_d (μM)	Efficiency ($\mu M^{-1}\ s^{-1}$)[b]	Discrimination[c]
dATP	220 ± 16	3.2 ± 0.7	69	
EFdA-TP	0.29 ± 0.02	18 ± 4	0.016	4,300

[a] At least 7 different time courses containing 10 time points each were used to generate k_{pol} and K_d. The standard error estimates shown were derived from the deviance from the nonlinear regression fits determined using KaleidaGraph software.
[b] Efficiency = k_{pol}/K_d.
[c] Discrimination = $\text{efficiency}_{(dATP)}/\text{efficiency}_{(EFdA\text{-}TP)}$.

with the very low incorporation rate and low affinity for EFdA indicates a very low risk of Pol γ-mediated toxicity.

This rare EFdA incorporation event can be further mitigated via excision by Pol γ. To measure the rate of excision (k_{exo}), WT HIV-1 RT (purified as described previously [6, 14]) incorporated a single EFdA-TP into a D21/D36 substrate (Fig. 1B) (11). Under single-turnover conditions, exonuclease-competent Pol γ holoenzyme (purification detailed elsewhere [23]) and the D21-EFdA/D36 substrate were manually mixed with magnesium chloride, followed by quenching and product separation (Fig. 3A) (28). A plot of the percent loss of substrate versus time was fit to a

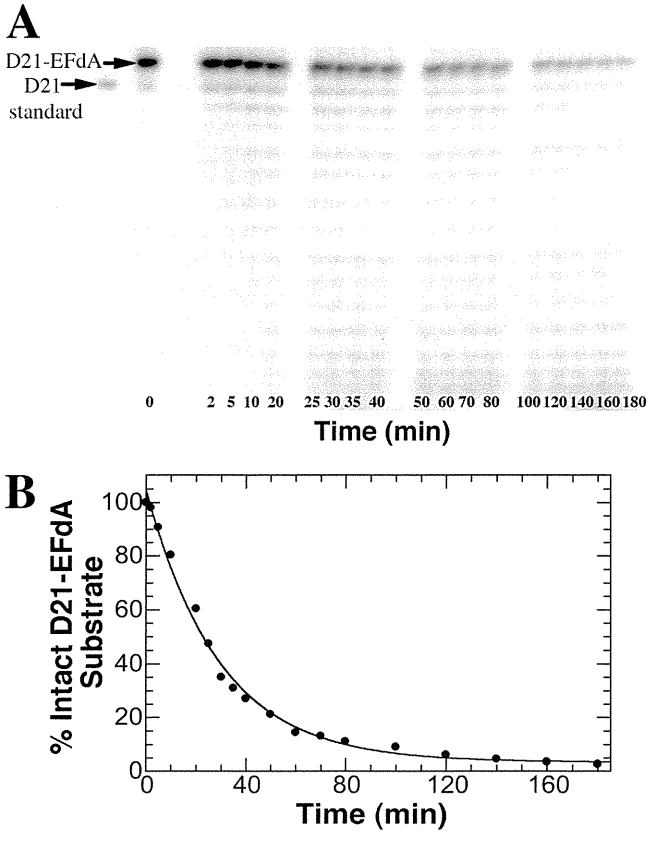

FIG 3 Excision of EFdA by Pol γ. (A) Gel analysis of the intact D21-EFdA substrate and degradation products over a 3-h time course. (B) A single exponential fitting of a plot of the percent loss of substrate versus time yielded a k_{exo} value of 0.00057 ± 0.00003 s^{-1}. Each point represents a single experiment within the time course, and the standard error associated with the k_{exo} value represents the deviance from this single exponential fitting as calculated by the KaleidaGraph software.

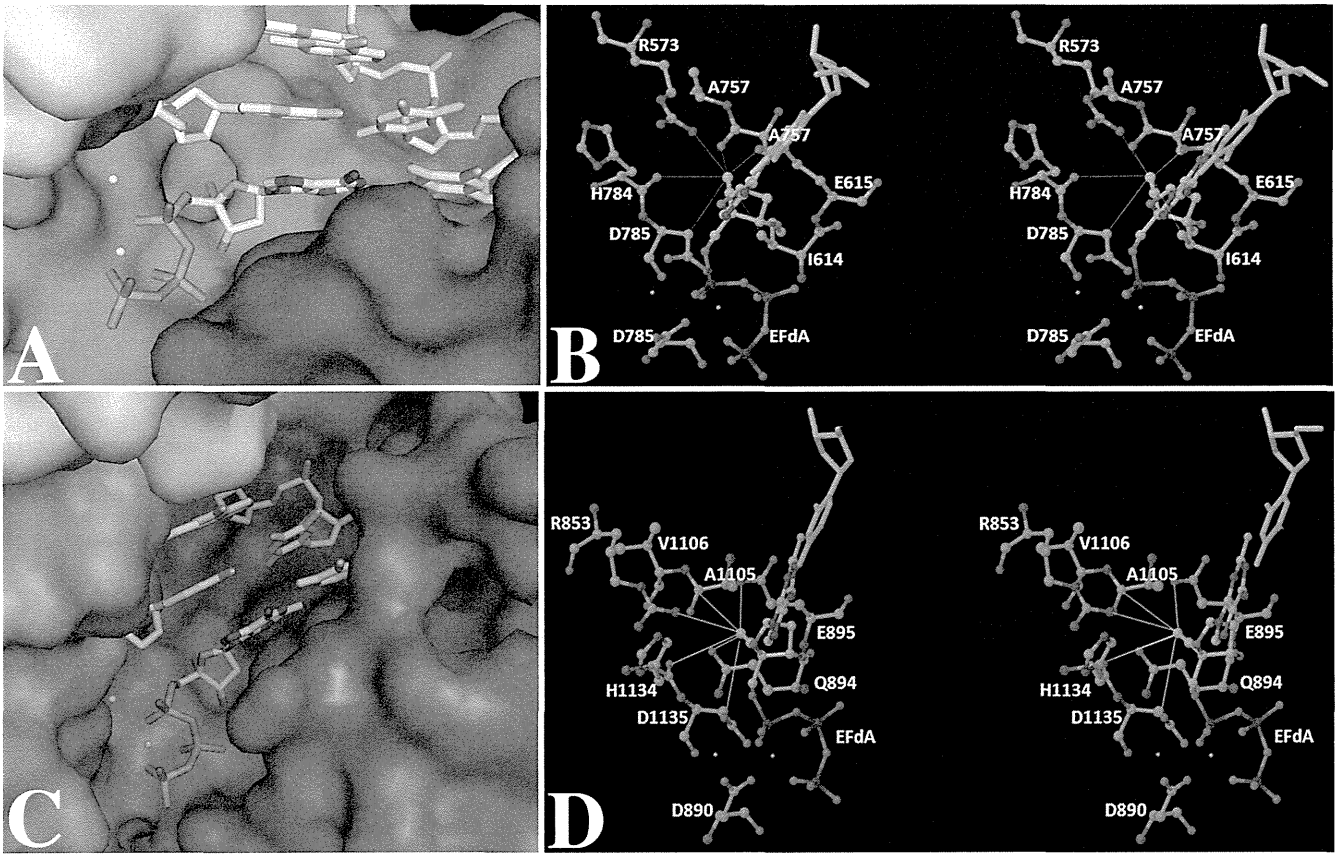

FIG 4 (A) KlenTaq–DNA–EFdA-TP. (B) KlenTaq–DNA–EFdA-TP in stereo view, highlighting interactions of the 4′-ethynyl group of EFdA-TP with the neighboring amino acid residues. (C) Pol γA–DNA–EFdA-TP. (D) Pol γA–DNA–EFdA-TP in stereo view, highlighting the interactions of 4′-ethynyl group of EfdA-TP with proximal amino acid residues. For (A) and (C), the ternary complex model of the polymerase subunit with template (cyan), primer (yellow), and EFdA-TP (colored by atom type as follows: carbon, gray; nitrogen, blue; oxygen, purple; phosphorous, orange). The enzyme is rendered as a Connolly surface representation with the thumb, palm, finger, and exonuclease domains colored in green, red, blue, and orange, respectively. For clear visualization of EFdA-TP, some residues at the tip of the fingers and thumb have been removed. However, these side chains were part of the computations. The metal ions are depicted as white spheres. For panels B and D, the amino acid residues (colored by atom type as follows: carbon, green; nitrogen, blue; oxygen, red) important for interaction with EFdA-TP (using the same color scheme, except carbon is colored gray and phosphorous purple) are highlighted. The template is shown in cyan. The thin lines depict the possible interactions with the amino acid residues in the vicinity of the 4′-ethynyl group of EFdA-TP. These interactions are not necessarily the hydrogen bonds. Interaction lengths range from 2.9 to 4 Å. Panels A and C were generated by PyMOL (http://www.pymol.org/), and panels B and D were generated by Maestro 9.1 (Schrödinger Inc., NY).

single exponential equation to generate k_{exo} (Fig. 3B). EFdA was excised at 0.00057 ± 0.00003 s^{-1}, yielding a half-life of ~20 min, similar to ddAMP removal (0.0005 s^{-1}) (11). Since DNA dissociates from Pol γ at 0.02 s^{-1} (10), it is likely that dissociation will occur before EFdA excision. The k_{exo} for EFdA falls in range of currently available NRTIs, 1.4-fold higher than for d4T and AZT (10) and much higher than for zalcitabine, which is too low to be detected (<0.00002 s^{-1}) (7), but 1.3-fold and 26-fold lower than for tenofovir (10) and lamivudine (7), respectively. Since dosages of EFdA are expected to be low due to the observed high potency, and because the Pol γ incorporation rate is very low with moderate EFdA excision rates, it is predicted that Pol γ-related toxicity will be limited. However, mitochondrial toxicity must be tested under clinical settings.

To probe the mechanism of the 4,300-fold increased efficiency of dATP incorporation over EFdA-TP, we used structural modeling to compare the dATP and EFdA-TP ternary complexes using the currently available Pol γ crystal structure (19). The active site residues of Pol γA are seen at topologically equivalent positions in other A family polymerases, including the large fragment of Pol I from *Thermus aquaticus* (KlenTaq), which has been reported with all four incoming ddNTPs (21). After superimposing Pol γA and KlenTaq using their active sites as a reference point, we docked 6 bp of DNA from the 3′ end of the primer, the ddATP, and two catalytic metal ions from the KlenTaq structure (PDB ID 1QSY [21]) into the Pol γ structure using Glide (Schrödinger Suite). Significant steric interactions involving residues M1057 to A1064, a region not found in other A family DNA polymerases (19), prevented energetically favorable docking of the template primer and ddATP at the Pol γA active site, and we deleted these residues because they are expected to undergo significant conformational changes in the ternary complex. Interestingly, similar changes are observed in N4 virion RNA polymerase, which undergoes a conformational change to displace a structurally equivalent region in order to accommodate duplex DNA (8).

The modeled KlenTaq–DNA–EFdA-TP ternary complex is shown in Fig. 4A and B for comparison with the Pol γA–DNA–EFdA-TP complex shown in Fig. 4C and D. The 4′-ethynyl group

of EFdA-TP is reasonably accommodated in a pocket defined by KlenTaq residues I614, E615, R753, and H784 (corresponding to Q894, E895, R853, and H1134 in Pol γ), which are 4.2, 3.5, 3.3, and 4.6 Å, respectively, away from this group, consistent with a relatively small change in affinity for EFdA-TP versus dATP (Table 1). A measureable K_i value (25 μM) has been determined for EFdA-TP (26), supporting the hypothesis that the binding pocket is similar for EFdA-TP and dATP. To probe this idea further, we employed a pre-steady-state competition assay in which the rate of dATP incorporation by the Pol γ holoenzyme was measured in the presence of various concentrations of EFdA-TP. EFdA-TP was able to compete with dATP for the binding pocket, as indicated by a linear decrease in the k_{obs}, although concentrations higher than the K_d for EFdA binding (18 μM) were required to lower the rate of incorporation of 3 μM dATP (the K_d of dATP) (data not shown). To achieve a 4.8-fold drop in the rate of dATP incorporation, a concentration of EFdA-TP at nearly 6 times its K_d was required (data not shown). Overall, this competition experiment supports our model of a similar binding pocket for EFdA-TP and dATP, leading to only minor changes in K_d, as well as our finding that EFdA-TP is a poor competitor of dATP due to its inefficient incorporation.

The 4′-ethynyl group of EFdA appears to be in the proximity of E895 in Pol γ (E615 in KlenTaq) and may disturb hydrogen bonding with Y955 (Y671 in KlenTaq), which is required for efficient catalysis in the Pol I family (Fig. 4). This may explain the severe defects in k_{pol} observed for EFdA incorporation. Interestingly, incorporation of 4′-alkyl-modified nucleoside analogs by the Klenow fragment of DNA Pol I from *Escherichia coli* showed a lower k_{pol} (~60-fold), with a small loss of affinity (~1.5-fold), similar to that for EFdA (5).

In summary, we have investigated the effects of a novel NRTI, EFdA, on Pol γ. EFdA has shown great promise in preclinical trials for the treatment of HIV infection because of its high potency and low toxicity. We show that this low toxicity is due in part to extremely inefficient EFdA incorporation and, to a lesser extent, subsequent EFdA excision by human Pol γ. Structural modeling suggests that the relatively small change in affinity for EFdA-TP relative to dATP is due to similar accommodation within a pocket, while the severe decrease in k_{pol} may be due to hydrogen bond disruption by EFdA. Characterizing the ability of Pol γ to incorporate NRTIs into a DNA template is critical to assess the safety of new drugs in this important class of antivirals.

ACKNOWLEDGMENTS

This work was supported by NIH grants R01 GM049551 (to K.S.A.), F32 GM099289 (to C.D.S.), AI094715, AI076119, AI079801, and AI074389 (to S.G.S.) and by the Intramural Research Program of the NIH, NIEHS, ES 065080 (to W.C.C.).

Additionally, C.D.S. and K.S.A. thank Ligong Wang and Krasimir Spasov for the purification of the Pol γ accessory subunit and RT, respectively.

REFERENCES

1. **Anderson JP, Daifuku R, Loeb LA.** 2004. Viral error catastrophe by mutagenic nucleosides. Annu. Rev. Microbiol. **58**:183–205.
2. **Brinkman K, Kakuda TN.** 2000. Mitochondrial toxicity of nucleoside analogue reverse transcriptase inhibitors: a looming obstacle for long-term antiretroviral therapy? Curr. Opin. Infect. Dis. **13**:5–11.
3. **Brinkman K, Smeitink JA, Romijn JA, Reiss P.** 1999. Mitochondrial toxicity induced by nucleoside-analogue reverse-transcriptase inhibitors is a key factor in the pathogenesis of antiretroviral-therapy-related lipodystrophy. Lancet **354**:1112–1115.
4. **Dalakas MC, et al.** 1990. Mitochondrial myopathy caused by long-term zidovudine therapy. N. Engl. J. Med. **322**:1098–1105.
5. **Di Pasquale F, et al.** 2008. Opposed steric constraints in human DNA polymerase beta and *E. coli* DNA polymerase I. J. Am. Chem. Soc. **130**: 10748–10757.
6. **Feng JY, Anderson KS.** 1999. Mechanistic studies comparing the incorporation of (+) and (-) isomers of 3TCTP by HIV-1 reverse transcriptase. Biochemistry **38**:55–63.
7. **Feng JY, Johnson AA, Johnson KA, Anderson KS.** 2001. Insights into the molecular mechanism of mitochondrial toxicity by AIDS drugs. J. Biol. Chem. **276**:23832–23837.
8. **Gleghorn ML, Davydova EK, Rothman-Denes LB, Murakami KS.** 2008. Structural basis for DNA-hairpin promoter recognition by the bacteriophage N4 virion RNA polymerase. Mol. Cell **32**:707–717.
9. **Hattori S, et al.** 2009. Potent activity of a nucleoside reverse transcriptase inhibitor, 4′-ethynyl-2-fluoro-2′-deoxyadenosine, against human immunodeficiency virus type 1 infection in a model using human peripheral blood mononuclear cell-transplanted NOD/SCID Janus kinase 3 knockout mice. Antimicrob. Agents Chemother. **53**:3887–3893.
10. **Johnson AA, Johnson KA.** 2001. Exonuclease proofreading by human mitochondrial DNA polymerase. J. Biol. Chem. **276**:38097–38107.
11. **Johnson AA, et al.** 2001. Toxicity of antiviral nucleoside analogs and the human mitochondrial DNA polymerase. J. Biol. Chem. **276**:40847–40857.
12. **Kakuda TN, Brundage RC, Anderson PL, Fletcher CV.** 1999. Nucleoside reverse transcriptase inhibitor-induced mitochondrial toxicity as an etiology for lipodystrophy. AIDS **13**:2311–2312.
13. **Kawamoto A, et al.** 2008. 2′-Deoxy-4′-*C*-ethynyl-2-halo-adenosines active against drug-resistant human immunodeficiency virus type 1 variants. Int. J. Biochem. Cell Biol. **40**:2410–2420.
14. **Kerr SG, Anderson KS.** 1997. RNA dependent DNA replication fidelity of HIV-1 reverse transcriptase: evidence of discrimination between DNA and RNA substrates. Biochemistry **36**:14056–14063.
15. **Kirby KA, et al.** 2011. The sugar ring conformation of 4′-ethynyl-2-fluoro-2′-deoxyadenosine and its recognition by the polymerase active site of HIV reverse transcriptase. Cell. Mol. Biol. (Noisy-le-grand) **57**:40–46.
16. **Koczor CA, Lewis W.** 2010. Nucleoside reverse transcriptase inhibitor toxicity and mitochondrial DNA. Expert Opin. Drug Metab. Toxicol. **6**:1493–1504.
17. **Kodama EI, et al.** 2001. 4′-Ethynyl nucleoside analogs: potent inhibitors of multidrug-resistant human immunodeficiency virus variants *in vitro*. Antimicrob. Agents Chemother. **45**:1539–1546.
18. **Kohler JJ, Lewis W.** 2007. A brief overview of mechanisms of mitochondrial toxicity from NRTIs. Environ. Mol. Mutagen. **48**:166–172.
19. **Lee YS, Kennedy WD, Yin YW.** 2009. Structural insight into processive human mitochondrial DNA synthesis and disease-related polymerase mutations. Cell **139**:312–324.
20. **Lewis W, Day BJ, Copeland WC.** 2003. Mitochondrial toxicity of NRTI antiviral drugs: an integrated cellular perspective. Nat. Rev. Drug Discov. **2**:812–822.
21. **Li Y, Kong Y, Korolev S, Waksman G.** 1998. Crystal structures of the Klenow fragment of *Thermus aquaticus* DNA polymerase I complexed with deoxyribonucleoside triphosphates. Protein Sci. **7**:1116–1123.
22. **Lim SE, Longley MJ, Copeland WC.** 1999. The mitochondrial p55 accessory subunit of human DNA polymerase gamma enhances DNA binding, promotes processive DNA synthesis, and confers *N*-ethylmaleimide resistance. J. Biol. Chem. **274**:38197–38203.
23. **Longley MJ, Ropp PA, Lim SE, Copeland WC.** 1998. Characterization of the native and recombinant catalytic subunit of human DNA polymerase gamma: identification of residues critical for exonuclease activity and dideoxynucleotide sensitivity. Biochemistry **37**:10529–10539.
24. **Michailidis E, et al.** 2009. Mechanism of inhibition of HIV-1 reverse transcriptase by 4′-ethynyl-2-fluoro-2′-deoxyadenosine triphosphate, a translocation-defective reverse transcriptase inhibitor. J. Biol. Chem. **284**: 35681–35691.
25. **Murakami E, Basavapathruni A, Bradley WD, Anderson KS.** 2005. Mechanism of action of a novel viral mutagenic covert nucleotide: molecular interactions with HIV-1 reverse transcriptase and host cell DNA polymerases. Antiviral Res. **67**:10–17.
26. **Nakata H, et al.** 2007. Activity against human immunodeficiency virus type 1, intracellular metabolism, and effects on human DNA polymerases

of 4′-ethynyl-2-fluoro-2′-deoxyadenosine. Antimicrob. Agents Chemother. 51:2701–2708.
27. **Ohrui H, et al.** 2007. 2′-Deoxy-4′-*C*-ethynyl-2-fluoroadenosine: a nucleoside reverse transcriptase inhibitor with highly potent activity against wide spectrum of HIV-1 strains, favorable toxic profiles, and stability in plasma. Nucleosides Nucleotides Nucleic Acids 26:1543–1546.
28. **Ray AS, et al.** 2007. Interaction of 2′-deoxyguanosine triphosphate analogue inhibitors of HIV reverse transcriptase with human mitochondrial DNA polymerase gamma. Antivir. Chem. Chemother. 18:25–33.
29. **Yakubovskaya E, Chen Z, Carrodeguas JA, Kisker C, Bogenhagen DF.** 2006. Functional human mitochondrial DNA polymerase gamma forms a heterotrimer. J. Biol. Chem. 281:374–382.

Published online 8 September 2011

Nucleic Acids Research, 2012, Vol. 40, No. 1 345–359
doi:10.1093/nar/gkr694

Biochemical, inhibition and inhibitor resistance studies of xenotropic murine leukemia virus-related virus reverse transcriptase

Tanyaradzwa P. Ndongwe[1], Adeyemi O. Adedeji[1], Eleftherios Michailidis[1], Yee Tsuey Ong[1], Atsuko Hachiya[1], Bruno Marchand[1], Emily M. Ryan[1], Devendra K. Rai[1], Karen A. Kirby[1], Angela S. Whatley[1], Donald H. Burke[1,2], Marc Johnson[1], Shilei Ding[3], Yi-Min Zheng[1], Shan-Lu Liu[1,3], Ei-Ichi Kodama[4], Krista A. Delviks-Frankenberry[5], Vinay K. Pathak[5], Hiroaki Mitsuya[6], Michael A. Parniak[7], Kamalendra Singh[1] and Stefan G. Sarafianos[1,2,*]

[1]Christopher Bond Life Sciences Center, Department of Molecular Microbiology & Immunology, University of Missouri, School of Medicine, Columbia, [2]Department of Biochemistry, University of Missouri, Columbia, MO 65211, USA, [3]Department of Microbiology and Immunology, McGill University, Montreal, QC, Canada, [4]Department of Internal Medicine, Division of Emerging Infectious Diseases, Tohoku University School of Medicine, Sendai, Japan, [5]HIV Drug Resistance Program, National Cancer Institute-Frederick, Frederick MD, [6]Department of Internal Medicine, Kumamoto University School of Medicine, Kumamoto Japan & Experimental Retrovirology Section, HIV/AIDS Malignancy Branch, NIH, Bethesda MD and [7]Department of Molecular Genetics & Biochemistry, University of Pittsburgh School of Medicine, Pittsburgh, PA, USA

Received June 3, 2011; Revised August 5, 2011; Accepted August 8, 2011

ABSTRACT

We report key mechanistic differences between the reverse transcriptases (RT) of human immunodeficiency virus type-1 (HIV-1) and of xenotropic murine leukemia virus-related virus (XMRV), a gammaretrovirus that can infect human cells. Steady and pre-steady state kinetics demonstrated that XMRV RT is significantly less efficient in DNA synthesis and in unblocking chain-terminated primers. Surface plasmon resonance experiments showed that the gammaretroviral enzyme has a remarkably higher dissociation rate (k_{off}) from DNA, which also results in lower processivity than HIV-1 RT. Transient kinetics of mismatch incorporation revealed that XMRV RT has higher fidelity than HIV-1 RT. We identified RNA aptamers that potently inhibit XMRV, but not HIV-1 RT. XMRV RT is highly susceptible to some nucleoside RT inhibitors, including Translocation Deficient RT inhibitors, but not to non-nucleoside RT inhibitors. We demonstrated that XMRV RT mutants K103R and Q190M, which are equivalent to HIV-1 mutants that are resistant to tenofovir (K65R) and AZT (Q151M), are also resistant to the respective drugs, suggesting that XMRV can acquire resistance to these compounds through the decreased incorporation mechanism reported in HIV-1.

INTRODUCTION

Xenotropic murine leukemia virus-related virus (XMRV) is a gammaretrovirus that was first identified in some prostate cancer tissues (1,2) While some subsequent reports confirmed the presence of XMRV in prostate cancer samples (3–6), several others found little or no evidence of the virus in patient samples (7–9). XMRV DNA was also reported in 67% of patients with chronic fatigue syndrome (CFS) (10), but several subsequent studies in Europe and the USA failed to identify XMRV DNA in CFS patients or healthy controls (11–15). Hence, the relevance of XMRV to human disease remains unclear (16) and have been challenged (17). Most recently, it has been reported that XMRV has been generated through recombination of two separate proviruses suggesting that the association of XMRV with human disease is due to contamination of human samples with virus originating from this recombination event (18). Nonetheless, as a retrovirus that can infect human cells, XMRV can be very helpful in advancing our understanding of the mechanisms of retroviral reverse transcription, inhibition and drug resistance.

*To whom correspondence should be addressed. Tel: +1 573 882 4338; Fax: +1 573 884 9676; Email: sarafianoss@missouri.edu

XMRV RT is similar to the Moloney murine leukemia virus (MoMLV) RT, which has been the subject of structural and biochemical studies (19–24). Most of the differences between these gammaretroviral enzymes are at the RNase H domain (Supplementary Figure S1). Comparisons of human immunodeficiency virus type-1 (HIV) RT with MoMLV RT have revealed structural and sequence differences (21). For example, HIV-1 RT is a heterodimer composed of two related subunits (25,26) [reviewed in (27,28)]. Its larger p66 subunit (~66 kDa) contains both the polymerase and RNase H domains; the smaller p51 subunit, (~51 kDa), is derived from the p66 subunit by proteolytic cleavage and its role is to provide structural support and optimize RT's biochemical functions (29). In contrast, structural studies have demonstrated that MoMLV RT is a monomer of about 74 kDa, although one study reported that it may form a homodimer during DNA synthesis (30). So far, there are no published biochemical or structural studies on XMRV RT. Hence, the present study on this enzyme and its comparison to related enzymes provides an excellent opportunity to advance our biochemical understanding of the mechanism of reverse transcription, its inhibition and drug resistance.

MATERIALS AND METHODS

Expression and purification of XMRV, HIV-1 and MoMLV RTs

The plasmid pBSK-XMRV containing the coding sequence of XMRV RT from the VP62 clone (GenBank: DQ399707.1) was chemically synthesized and optimized for bacterial expression by Epoch Biolabs Inc (Missouri City, Texas, USA). The 2013 bp XMRV RT sequence was amplified from pBSK-XMRVRT by PCR, using the forward and reverse primers 1 (all primer sequences are shown in Supplementary Table S1), resulting in NdeI and HindIII restriction sites. Drug resistant XMRV RT mutants Q190M and K103R (equivalent to HIV-1 Q151M RT and K65R) were generated by site-directed mutagenesis using forward and reverse primers 2 and 3. The digested amplicons were ligated into pET-28a (Novagen), resulting into a construct that expresses an N-terminal hexahistidine tag. pET-28a-MRT encoding full-length wild-type MoMLV RT was provided by Dr M. Modak (New Jersey Medical School, Newark NJ, USA).

Expression and purification of MoMLV and XMRV RTs were carried out similarly to our previously published protocols (23,24). Briefly, RTs were expressed in BL21-pLysS *Escherichia coli* (Invitrogen) grown at 37°C and induced with 150 μM IPTG at OD_{600} 0.8, followed by 16 h growth at 17°C. A cell pellet from a 3 l culture was incubated with 40 ml lysis buffer (50 mM Tris–HCl, pH 7.8, 500 mM NaCl, 1 mM PMSF, 0.1% NP-40, 1% sucrose and 2 mg/ml lysozyme), then sonicated and centrifuged at 15,000 *g* for 30 min. The supernatant was diluted 2-fold in Buffer A (50 mM Tri–HCl pH 7.8, 1 mM PMSF, 4% streptomycin sulfate and 10% sucrose), stirred on ice for 30 min and centrifuged. The supernatant was loaded on a Ni-NTA column and bound proteins were washed with 20 ml Buffer B (20 mM Tris–HCl pH 7.5, 500 mM NaCl) and 5 mM imidazole, followed by 20 ml Buffer B with 75 mM imidazole. RT was eluted in 2 ml fractions with 20 ml buffer B containing 300 mM imidazole. Fractions with RT were pooled and further purified by size exclusion chromatography (Superdex 75; GE Healthcare). RTs (>95% pure) were stored in 50 mM Tris–HCl pH 7.0, 100 mM NaCl, 1 mM DTT, 0.1% NP-40 and 30% glycerol in 10 μl aliquots at −20°C. Protein concentrations were determined by measuring UV_{280} (molar extinction coefficients of 106 and 103 $M^{-1}cm^{-1}$ for XMRV and MoMLV RT).

HIV-1 RT was cloned in a pETduo vector and purified as described previously (29,31,32). Oligonucleotide sequences (IDT-Coralville, IA, USA) of DNA/RNA substrates are shown in Supplementary Table S1. Nucleotides were purchased from Fermentas (Glen Burnie, MD, USA). They were treated with inorganic pyrophosphatase (Roche Diagnostics, Mannheim, Germany) as described previously (33) to remove PPi that might interfere with excision assays.

Steady state kinetics

Steady state parameters K_m and k_{cat} for dATP incorporation were determined using single nucleotide incorporation gel-based assays. XMRV RT and MoMLV RT reactions were carried out in 50 mM Tris–HCl pH 7.8, 60 mM KCl, 0.1 mM DTT, 0.01% NP-40 and 0.01% bovine serum albumin (BSA) (Reaction Buffer) with 6 mM $MgCl_2$ or 1.5 mM $MnCl_2$, 0.5 mM EDTA, 200 nM or 100 nM T_{d26}/5′-Cy3-P_{d18b}, 20 nM or 5 nM RT for XMRV and MoMLV RTs, respectively and varying concentrations of dNTP in a final volume of 10 μl. The reactions for HIV-1 RT were carried out in Reaction Buffer with 100 nM T_{d26}/5′-Cy3-P_{d18b}, 10 nM HIV-1 RT and 6 mM $MgCl_2$ in a 20 μl reaction. All the concentrations mentioned here and in subsequent assays reflect final concentration of reactants otherwise mentioned reactions were stopped after 15 min for XMRV, 4 min for MoMLV RT, and 2.5 min for HIV-1. The products were resolved on 15% polyacrylamide–7M urea gels. The gels were scanned with a Fuji Fla-5000 PhosphorImager (Stamford, CT, USA) and the bands were quantified using MultiGauge. Results were plotted using GraphPad Prism 4. K_m and k_{cat} were determined graphically using Michaelis–Menten equation.

Gel mobility shift assays

Formation of RT-DNA binary complex: 20 nM T_{d31}/5′-Cy3-P_{d18a} (Supplementary Table S1) was incubated for 10 minutes with increasing amounts of MoMLV or XMRV RT in 50 mM Tris–HCl pH 7.8, 0.01% BSA, 5 mM $MgCl_2$ and 10% (v/v) sucrose. The complexes were resolved on native 6% polyacrylamide 50 mM Tris–borate gel and visualized as described above.

Active site titration and determination of $K_{D.DNA}$

Active site concentrations and kinetic constants of DNA binding for XMRV, HIV-1 and MoMLV RTs were determined using pre-steady state experiments. Reactions

with XMRV and MoMLV RTs were carried out in the reaction buffers listed above. For XMRV RT 100 nM protein was pre-incubated with increasing concentrations of T_{d31}/5′-Cy3-P_{d18a}, followed by rapid mixing with a reaction mixture containing 5 mM $MgCl_2$ and 100 μM next incoming nucleotide (dATP). The reactions were quenched at various times (5 ms to 4 s) by adding EDTA to a final concentration of 50 mM. The amounts of 19-mer product were quantified and plotted against time. The data were fit to the following burst equation:

$$P = A(1 - e^{-k_{obs}t}) + k_{ss}t \quad (1)$$

where A is the amplitude of the burst phase that represents the RT–DNA complex at the start of the reaction, k_{obs} is the observed burst rate constant for dNTP incorporation, k_{ss} is the steady state rate constant and t is the reaction time. The rate constant of the linear phase (k_{cat}) was estimated by dividing the slope of the linear phase by the enzyme concentration. The active site concentration and T/P binding affinity ($K_{D.DNA}$) were determined by plotting the amplitude (A) against the concentration of T/P. Data were fit to the quadratic equation (Equation 2) using non-linear regression:

$$A = 0.5(K_D + [RT] + [DNA] - \sqrt{0.25(K_D + [RT] + [DNA])^2} - ([RT] + [DNA]) \quad (2)$$

where K_D is the dissociation constant for the RT–DNA complex, and [RT] is the concentration of active polymerase. HIV-1 RT's DNA binding affinity was determined as previously described (29).

Surface plasmon resonance assay

We used surface plasmon resonance (SPR) to measure the binding constants of XMRV and HIV-1 RTs to double-stranded DNA. Experiments were carried out using a Biacore T100 (GE Healthcare). To prepare the sensor chip surface we used the 5′-biotin-T_{d37}/P_{d25} oligonucleotide (Supplementary Table S1). One hundred and twenty RUs of this DNA duplex were bound in channel 2 of a streptavidin-coated sensor chip [Series S Sensor Chip SA (certified)] by flowing a solution of 0.1 μM DNA at a flow rate of 10 μl/min in a buffer containing 50 mM Tris pH 7.8, 50 mM NaCl. The binding constants were determined as follows: RT binding was observed by flowing solutions containing increasing concentrations of the enzyme (0.2, 0.5, 1, 2, 5, 10, 20, 50, 100 and 200 nM) in 50 mM Tris pH 7.8, 60 mM KCl, 1 mM DTT, 0.01% NP40 and 10 mM $MgCl_2$ in channels 1 (background) and 2 (test sample) at 30 μl/min. The trace obtained in channel 1 was subtracted from the trace in channel 2 to obtain the binding signal of RT. This signal was analyzed using the Biacore T100 Evaluation software to determine $K_{D.DNA}$, k_{on} and k_{off}.

Pre-steady state kinetics of dNTP incorporation

The optimal nucleotide incorporation rates (k_{pol}) were obtained by pre-steady state kinetics analysis using single nucleotide incorporation assays. A solution containing XMRV RT (150 nM final concentration) and T_{d31}/5′-Cy3-P_{d18a} (40 nM) was rapidly mixed with a solution of $MgCl_2$ (5 mM) and varying dATP (5–200 μM) for 0.1 to 6 s before quenching with EDTA (50 mM) (all concentrations in parentheses are final, unless otherwise stated). Products were resolved and quantified as described above. Burst phase incorporation rates and substrate affinities were obtained from fitting the data to Equation 1. Turnover rates (k_{pol}), dNTP binding to the RT-DNA complex ($K_{d.dATP}$), and observed burst rates (k_{obs}) were fit to the hyperbolic equation:

$$k_{obs} = (k_{pol}[dNTP])/(K_{d.dNTP} + [dNTP]) \quad (3)$$

HIV-1 RT's DNA binding affinity was determined as previously described (29).

Fidelity of DNA synthesis

The fidelity (error-proneness) of XMRV RT was determined and compared with that of MoMLV RT and HIV-1 RT by primer extension assays using 10 nM heteropolymeric T_{d100}/5′-Cy3-P_{d18a}. Reactions (10 μl) were carried out in Reaction Buffer containing all four dNTPs (100 μM each) or only three dNTPs (missing either dATP, dGTP or dTTP) at 100 μM each. Incubations of the XMRV and MoMLV (50 nM) reactions were at 37°C for 45 min and 30 min for HIV-1 RT (20 nM). Reactions were initiated by adding dNTPs, stopped with equal volume of formamide-bromophenol blue, and an aliquot was run on a 16% polyacrylamide–7M urea gel.

Kinetics of mismatch incorporation

For these experiments, instead of including the next correct nucleotide (dATP) in the polymerase reactions, we used dTTP as the mismatched incoming nucleotide. Hence, 50 nM XMRV RT was pre-incubated with 35 nM T_{d31}/5′-Cy3-P_{d18a} in reaction mixture. Reactions were initiated by adding dTTP (5–750 μM) and 5 mM $MgCl_2$, followed by incubation (37°C) for 5 min, due to the decreased mismatch incorporation rate of XMRV. For MoMLV RT, 30 nM RT and 20 nM DNA used and the reactions were carried out for 2.5 minutes. For HIV-1, 30 nM RT, 20 nM DNA and 0–200 μM nucleotide were used and the reactions were carried out for 2.5 min. The amount of extended primer was quantified and plotted against the concentration of dTTP. The data were used to derive the $K_{d.dNTP}$ of incorrect nucleotide binding, the rate k_{pol} (using Equations 1 and 3) and the efficiency of the misincorporation reaction ($k_{pol}/K_{d.dTTP}$).

Determination of *in vivo* fidelity

ANGIE P cells, which contain a retroviral vector (GA-1) that encodes a bacterial β-galactosidase gene (*lacZ*) and a neomycin phosphotransferase gene, were plated (5×10^6 cells/100 mm dish) and after 24 h were transfected using the calcium phosphate precipitation method with a plasmid expressing either XMRV or amphotropic MLV (AM-MLV) (three independent transfections per vector). After 48 h, the culture medium with XMRV or (AM-MLV) was harvested, serially diluted and used to infect

D17 target cells (2×10^5 cells/60 mm dish) in the presence of polybrene. The infected D17 cells were selected for resistance to G418 (400 μg/ml) in the presence of 1 μM AZT to suppress reinfection, and characterized by staining with 5-bromo-4-chloro-3-indoyl-β-D-galacto-pyranoside (X-Gal) ~2 weeks after G418 selection. The frequencies of inactivating mutations in *lacZ* quantified as described before (blue versus white colonies) (34).

Processivity of DNA synthesis—trap assay

Processivity reactions were carried out in Reaction Buffer containing 20 nM T_{d100}/P_{d18}, 100 μM of each dNTP, 30 nM HIV-1 RT, 50 nM MoMLV RT or 100 nM XMRV RT and 1 μg/μl unlabeled calf thymus DNA trap in 50 μL. Enzymes were pre-incubated with T_{d100}/P_{d18} for 1 min before adding dNTPs (100 μM each) together with the calf thymus DNA trap. Reactions were incubated at 37°C, and 10 μl aliquots were taken out at 3, 7.5 and 15 min for HIV-1 RT or at 7.5, 15 and 30 min for XMRV RT and MoMLV RT, and mixed with equal volume of loading dye. The effectiveness of the trap was determined by pre-incubating the enzyme with the trap before adding T_{d100}/P_{d18}. Control DNA synthesis was measured in absence of trap under the same conditions. Reaction products were resolved as above.

Single turnover processivity assays

Thirty nanomolar $T_{d31}/5'$-Cy3-P_{d18a} was pre-incubated for 10 min with 100 nM XMRV or 50 nM MoMLV RT in Reaction Buffer, then rapidly mixed with 100 μM dNTPs, 5 mM $MgCl_2$ for varying times (0.1–45 s) before quenching with EDTA (50 mM final). Single turnover processivity of HIV-1 RT was assayed with 40 nM enzyme, 20 nM DNA and 50 μM of each nucleotide were used. The reaction products were resolved and quantified as described above. The data were fit to a one-phase exponential decay equation for the elongation of the 18-mer primer. The rates of appearance and extension of products from subsequent nucleotide incorporations (19- and 27-mer) were obtained by fitting the intensities of corresponding bands to double exponential (Equation 4):

$$P = A(1 - e^{-k_1 t}) + (e^{-k_2 t}) + C \quad (4)$$

where A is the amplitude, P is the amount of 19-mer, 20-mer or higher length products, k_1 is the rate of product generation, k_2 the rate of subsequent elongation and C a constant (29,35).

Assays for reverse transcriptase inhibition

DNA synthesis by 50 nM XMRV RT or MoMLV RT was carried out in Reaction Buffer using 20 nM $T_{d100}/5'$-Cy3-P_{d18a}, 2.5 μM dNTP, 5 mM $MgCl_2$ and varying amounts of NRTI (0–100 μM). Reactions were quenched with 95% formamide after 1 h incubation at 37°C (38). In experiments with aptamers 10 nM XMRV RT, 20 nM $T_{d31}/5'$-Cy3-P_{d18a} and 50 μM dNTPs were used in the presence of varying amounts of aptamer for 30 min (0–500 nM for m.1.3; 0–25 nM for m.1.4 and m.1.1FL). The inhibition of DNA polymerization was monitored by resolving the products on 15% polyacrylamide–7 M urea gels and visualized as described above. Bands corresponding to full extension products were quantified using MultiGauge Software and IC_{50}s were obtained from dose–response curves using GraphPad Prism.

PPi- and ATP-dependent excision and rescue of $T/P_{AZT\text{-}MP}$ or $T/P_{EFdA\text{-}MP}$

The ability of enzymes to use PPi or ATP to unblock template-primers that had AZT-MP ($T/P_{AZT\text{-}MP}$) or EFdA-MP ($T/P_{EFdA\text{-}MP}$) at their 3′ primer ends was measured as follows: 20 nM of $T/P_{AZT\text{-}MP}$ or $T/P_{EFdA\text{-}MP}$ were prepared as described before (32). They were incubated at 37°C with either 60 nM HIV-1 RT or 200 nM XMRV RT in the presence of 0.15 mM PPi or 3.5 mM ATP for PPi- or ATP-dependent rescue reactions, respectively. Reactions were initiated by the addition of $MgCl_2$ (6 mM). Aliquots were removed at different times (0–90 min) and analyzed as above. Rescue assays were performed in the presence of 100 μM dATP to prevent EFdA-MP reincorporation, 0.5 μM dTTP, 10 μM ddGTP and 10 mM $MgCl_2$.

Molecular modeling

The sequence of XMRV RT from the VP62 clone was aligned with that of MoMLV RT (PDB: 1RW3) (21,22) using ClustalW. To generate the homology model of XMRV RT, we used the Prime protocol of the Schrödinger software suite (Schrödinger Inc. NY). The resulting molecular model was further energy minimized by OPLS2005 force field using the Impact option of Schrödinger. The final model was validated with PROCHECK v.3.5.4.

RESULTS

Comparison of RT sequences

The XMRV and MoMLV enzymes are closely related (~95% sequence identity) with most of the differences between them being in the RNase H domain (Supplementary Figure S1). While XMRV and MoMLV differ significantly from HIV-1 RT, the known polymerase motifs (A–F) are well conserved in all three enzymes (Supplementary Figure S1). Specifically, the active site aspartates in Motifs A and C (Figure 9) (D150, D224, D225 in XMRV RT; D150, D224, D225 in MoMLV RT; D110, D185, D186 in HIV-1 RT) are conserved in all three RTs. Also, the three enzymes are similar in Motif B, which is involved in dNTP binding and multidrug resistance (AZT and dideoxy-nucleoside drugs) through the decreased incorporation mechanism (27,39–41). Specifically, all three enzymes have a glutamine at the start of this motif (Q151 in HIV-1 RT, Q190 in XMRV RT and Q190 in MoMLV RT). Motif D includes HIV-1 RT residues L210 and T215, which when mutated they enhance excision of AZT from the AZT-terminated primer terminus. This motif is mostly different in XMRV and MoMLV RTs, where the corresponding residues are N226 and A231 (Supplementary Figure S1). K219 of HIV-1 RT Motif D is proximal to

the dNTP-binding pocket and is also conserved in the other enzymes (K235). The DNA primer grip (Motif E) (36,42) in HIV-1 RT ($M_{230}G_{231}Y_{232}$) is slightly different in the gammaretroviral enzymes ($L_{245}G_{246}Y_{247}$). Motif F at the fingers subdomain of all enzymes has two conserved lysines that bind the triphosphate of the dNTP (K65 and K72 in HIV-1 RT; K103 and K110 in XMRV and MoMLV RTs).

Several HIV-1 residues involved in NRTI resistance have the resistance mutations in XMRV and MoMLV RTs (Table 1). Hence, XMRV and MoMLV RTs have a Val as the X residue (codon 223) of the conserved YXDD sequence of Motif C. An M184V mutation at this position in HIV-1 RT causes strong, steric hindrance-based, resistance to 3TC and FTC (43–45), and to a lesser extent to ddI, ABC [reviewed in (46)], and translocation defective RT inhibitors (TDRTIs) (43) (Table 1). Similarly, the M41L mutation, which causes excision-based AZT resistance in HIV is already present in XMRV and MoMLV RT (L81, Table 1). The gammaretroviral enzymes differ from HIV-1 RT in several other HIV drug resistance sites (HIV residues 62, 67, 69, 70, 75, 77, 115, 210, 215) (Table 1). Finally, there are also differences in residues that are essential for NNRTI binding in HIV-1 RT: W229 changes to Y268 in XMRV RT, Y181 to L220, Y188 to L227 and G190 to A229 (Table 1) (27,28,47–49).

Preparation of MoMLV and XMRV RTs

The sequence coding for full-length XMRV RT from the VP-62 clone (NCBI RefSeq: NC_007815) (1) was optimized for expression in bacteria, synthesized by Epoch Biolabs and cloned as described in 'Materials and Methods' section. Both XMRV RT and MoMLV RT were tagged with a hexahistidine sequence at the N-terminus and expressed with a yield of ~2 mg/l of culture. Purified enzymes (>95% pure, Supplementary Figure S2) were stored at −20°C. The presence of NP-40 or glycerol was critical for enzyme stability.

Steady state kinetics of nucleotide incorporation

Initial polymerase activity assays using T_{d31}/5′-Cy3-P_{d18a} displayed overall slower polymerase activity of XMRV RT compared to HIV-1 and MoMLV RTs. This observation led us to investigate the steady state nucleotide incorporation properties of XMRV RT using single nucleotide incorporation assays. The estimated values for k_{cat} (19.9 min^{-1} for HIV-1 RT (32), 3.3 min^{-1} for MoMLV RT, 0.6 min^{-1} for XMRV RT) and $K_{m.dNTP}$ (0.07 μM for HIV-1 RT (32), 3.3 μM for MoMLV RT, 3.0 μM for XMRV RT) show that XMRV RT has a drastically reduced efficacy ($k_{cat}/K_{m.dNTP}$) at nucleotide incorporation, compared to both MoMLV and HIV-1 RTs.

DNA binding affinity

To assess if the efficiency of XMRV RT was also affected by a lower DNA binding affinity we measured the DNA binding affinity of the enzymes using three methods: gel-mobility shift assays, pre-steady state kinetics and SPR. Gel-mobility shift assays showed that the $K_{D.DNA}$ for XMRV RT was marginally higher than that for HIV-1 RT and MoMLV RT (data not shown) (50) suggesting weaker binding to DNA.

DNA binding affinity using pre-steady state kinetics

Pre-steady state kinetics allows estimation of the fraction of active polymerase sites as well as the $K_{D.DNA}$ value for the enzyme. The amplitudes of DNA extensions using XMRV RT and/or MoMLV RT at varying DNA concentrations were plotted against the DNA concentration and

Table 1. HIV-1 RT drug resistance mutations with wild-type XMRV RT and MoMLV RT residues

	HIV-1 residue numbers	HIV-1 RT wt	HIV-1 resistance mutations					XMRV RT wt	MoMLV RT wt
			3TC	ABC	TDF	D4T	EFdA		
Thymidine analog mutations (TAMs)	184	M	V	V	–	–	V	V223	V223
	41	M	–	L	L	L	–	L81	L81
	67	D	–	N	N	N	–	G105	G105
	210	L	–	W	W	W	–	N226	N226
	215	T	–	FY	FY	FY	–	A231	A231
	219	K	–			QE	–	K235	K235
Non-thymidine analog regimen mutations	65	K	RN	RN	RN	RN	–	K103	K103
	70	K	EG	EG	EG	–	–	D108	D108
	74	L	–	VI	–	–	–	V112	V112
	75	V	–	TM	M	TM	–	Q113	Q113
	115	Y	–	F	F		–	F155	F155
	69	T	Ins	Ins	Ins	Ins	–	N107	N107
Multi-NRTI resistance mutations	151	Q	M	M	M	M	–	Q190	Q190
	62	A	V	V	V	V	–	P104	P104
	75	V	–	I	–	I	–	Q113	Q113
	77	F	–	L	–	L	–	L115	L115
	116	F	–	Y	–	Y	–	F156	F156
TDRTI Mutations	184	M	V	V	–	–	V	V223	V223
	165	T	–	–	–	–	R	H204	H204

The HIV-1 RT data are based on data from the Stanford HIV Database (85).
wt = wild-type.

the data were fit to the quadratic equation (Equation 2), yielding a $K_{D.DNA}$ of 33 nM for XMRV RT, 19 nM for MoMLV RT (Table 2) and 12.5 nM for HIV-1 RT (32). These values did not change significantly when tested with DNA of different lengths (data not shown). Hence, the transient kinetic experiments confirmed the findings of the gel-mobility shift assays showing XMRV RT to have lower DNA binding affinity than HIV-1 RT.

Binding kinetics of XMRV and HIV-1 RT to double-stranded DNA

Measurements of $K_{D.DNA}$ using gel-mobility shift assays and pre-steady state kinetic methods do not offer insights regarding the kinetics of binding and release of nucleic acid from the viral polymerases. Hence, we used SPR to measure directly DNA binding and the DNA dissociation components of the $K_{D.DNA}$. We attached on the SPR chip a nucleic acid biotinylated at the 5′ template end and immobilized it on a streptavidin sensor chip. Various concentrations of either XMRV or HIV-1 RT were flowed over the chip to measure the association (k_{on}) and dissociation (k_{off}) rates of the enzymes in real time (Figure 1). HIV-1 RT had considerably slower dissociation rates than XMRV RT, and longer dissociation phases were needed to obtain reliable values.

Several methods were tested to best fit our data. The 'heterogeneous ligand' method gave the best fit for both XMRV and HIV-1 RT. In this model the x^2 values for DNA binding to XMRV and HIV-1 RT were 9.3 RU^2 and 48.1 RU^2, respectively, compared to 15.1 RU^2 and 152 RU^2 when we tried fitting the data in a 'homogeneous ligand' model. The former model assumes that RT binds DNA in two different modes and provides two association (k_{on}) and two dissociation constants (k_{off}).

Our data show that XMRV RT has a slightly faster rate of association (k_{on}) than HIV-1 RT. We measured two k_{on} values of $7.3 \times 10^6 M^{-1}s^{-1}$ and $8.2 \times 10^4 M^{-1}s^{-1}$ for XMRV RT versus $7.6 \times 10^5 M^{-1}s^{-1}$ and $1.2 \times 10^6 M^{-1}s^{-1}$ for HIV-1 RT. Interestingly, the dissociation rate of XMRV RT was significantly faster than that of HIV-1 RT ($0.28\,s^{-1}$ and $0.0045\,s^{-1}$ for XMRV RT and 7.8×10^{-4} $s^{-1}$and $0.0076\,s^{-1}$ for HIV-1 RT) (Table 3). This difference in dissociation rate resulted in a $K_{D.DNA}$ at least 1 order of magnitude higher for XMRV RT compared to HIV-1 RT (38 and 54 nM versus 1.0 and 6.1 nM for XMRV and HIV-1 RT, respectively) (Table 3).

Table 2. Kinetic parameters of DNA binding and synthesis by HIV-1 and XMRV RTs

Nucleotide affinity and incorporation	HIV-1 RT[a]	MoMLV RT	XMRV RT
$K_{d.dNTP}$ (μM)	1.3 ± 0.4	25 ± 5.3	26.6 ± 6.5
k_{pol} (s^{-1})	24.4 ± 0.9	14.1 ± 0.8	8.9 ± 0.6
$k_{pol}/K_{d.dNTP}$ ($s^{-1}\cdot\mu M^{-1}$)	18.8	0.56	0.33
DNA binding affinity:			
$K_{D.DNA}$ (nM)	12.5	19.0	32.5

[a]HIV-1 RT data published previously (29).

Nucleotide binding affinity and optimal incorporation efficiency

A transient-state kinetics approach was used to estimate the dNTP binding affinity ($K_{d.dNTP}$) and maximum nucleotide incorporation rate (k_{pol}) (55). The rates at varying concentrations of next incoming nucleotide (dATP) were determined by plotting the amount of extended primer as a function of time. The rates were then plotted against dATP concentration. The data were fit to a hyperbola (Equation 3). The $K_{d.dNTP}$ for XMRV RT is 26.6 μM and the k_{pol} is $8.9\,s^{-1}$ (Figure 2) (Table 2). Under similar conditions the $K_{d.dNTP}$ and k_{pol} were 1.3 μM and $24.4\,s^{-1}$ for HIV-1 RT (29) and 25 μM and $14.1\,s^{-1}$ for MoMLV RT.

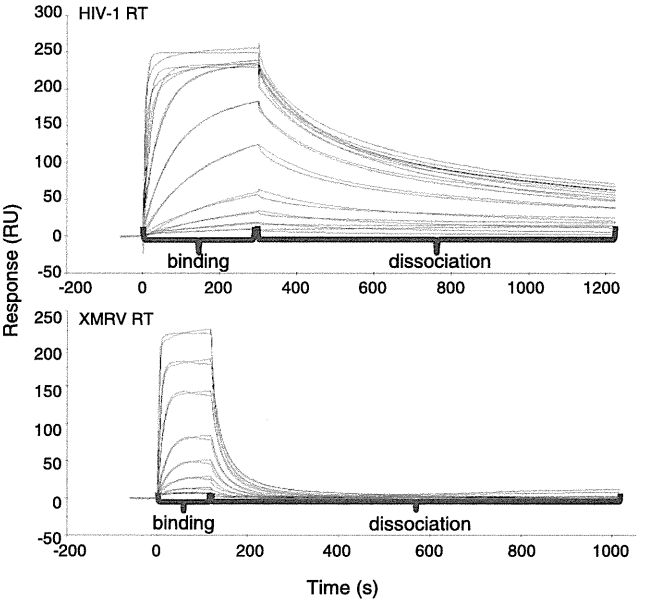

Figure 1. Assessment of $K_{D.DNA}$, k_{on} and k_{off} using surface plasmon resonance. SPR was used to measure the binding affinity of RTs to a nucleic acid substrate. Increasing concentrations of each RT (0.2, 0.5, 1, 2, 5, 10, 20, 50, 100 and 200 nM) were injected over a streptavidin chip with biotinylated double-stranded DNA immobilized on its surface as described in 'Materials and Methods' section. The experimental trace (red) shown is the result of a subtraction of the data obtained from the channel containing the immobilized nucleic acid minus the signal obtained from an empty channel. The black curve represents the fitted data according to the 'heterogeneous ligand' model that assumes two different binding modes for RT on the nucleic acid.

Table 3. DNA binding constants for HIV-1 and XMRV RTs from surface plasmon resonance

	HIV-1 RT	XMRV RT
k_{on} ($M^{-1}.s^{-1}$)	7.6×10^5	7.3×10^6
k_{off} (s^{-1})	7.8×10^{-4}	2.8×10^{-1}
$K_{D.DNA1}$ (nM)	1	38 (38-fold)[a]
k_{on} ($M^{-1}.s^{-1}$)	1.2×10^6	8.2×10^4
k_{off} (s^{-1})	7.6×10^{-3}	4.5×10^{-3}
$K_{D.DNA2}$ (nM)	6.1	54 (9-fold)[a]

[a]Increase in $K_{D.DNA}$ (decrease in affinity) with respect to HIV-1 RT. ($K_{D1\text{-}XMRV\ RT}/K_{D1HIV\text{-}1\text{-}RT}$ and $K_{D2\text{-}XMRV\ RT}/K_{D2HIV\text{-}1\text{-}RT}$).

Fidelity of nucleotide incorporation

To assess whether XMRV RT displays high nucleotide incorporation fidelity we monitored the incorporation of three dNTPs by XMRV RT and compared with HIV-1 RT (52). The results of fidelity assay are shown in Figure 3. The lanes marked '4dNTPs' for all enzymes represent the DNA synthesis using a T_{d100}/5′-Cy3-P_{d18a} template-primer in the presence of all four dNTPs. The subsequent lanes, marked '-dNTP', correspond to the synthesis of DNA in the absence of that specific deoxynucleotide triphosphate. The comparison of the DNA synthesis in the absence of one nucleotide by HIV-1 RT, MoMLV RT and XMRV RT shows that HIV-1 and MoMLV RTs were able to misincorporate and extend the primer beyond the missing nucleotide more efficiently than XMRV RT, suggesting that the latter is a less error prone DNA polymerase. It should be noted that the higher fidelity of XMRV is not the result of measuring a smaller number of errors because of the decreased replication rate, as the assay conditions were optimized to allow production of the same amount of full length product in the presence of all four dNTPs for and MoMLV RTs. To further investigate the fidelity of DNA synthesis by XMRV RT, the kinetics of mismatch nucleotide incorporation were carried out in a quantitative manner by monitoring the incorporation of single mismatched nucleotide under pre-steady state conditions. The estimated $K_{D.dTTP}$ (mismatch) and k_{pol} values show that XMRV RT has a lower affinity for a mismatched nucleotide but comparable turnover number than MoMLV RT, suggesting that the observed higher fidelity over MoMLV RT is due to differences during the nucleotide-binding step (Table 4). However, compared to HIV-1 RT, XMRV RT has decreased both affinity and incorporation rate, suggesting that its higher fidelity is the result of both decreased binding of mismatched nucleotides and slow rate of incorporation.

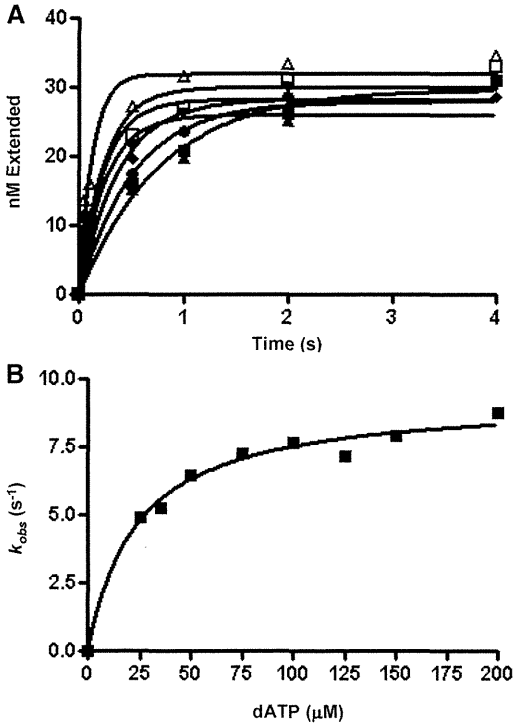

Figure 2. Pre-steady state kinetics of nucleotide incorporation by XMRV RT. 150 nM XMRV RT was pre-incubated with 40 nM T_{d31}/5′-Cy3-P_{d18a} rapidly mixed with a solution containing $MgCl_2$ (5 mM) and varying concentrations of dATP: 25 μM (filled square), 35 μM (filled triangle), 50 μM (filled inverted triangle), 75 μM (filled rhombus), 100 μM (filled circle), 125 μM (open square) and 150 μM (open triangle); and incubated for 0.1 to 6 s before being quenched with EDTA. The DNA product for each dATP concentration was fit to the burst equation (**A**). The burst amplitudes generated for each dATP concentration were then fit to a hyperbola equation (**B**) yielding the optimal rates of dNTP incorporation; k_{pol} (8.9 s^{-1}) and dNTP binding to the RT-DNA complex; $K_{d.dATP}$ (26.6 μM).

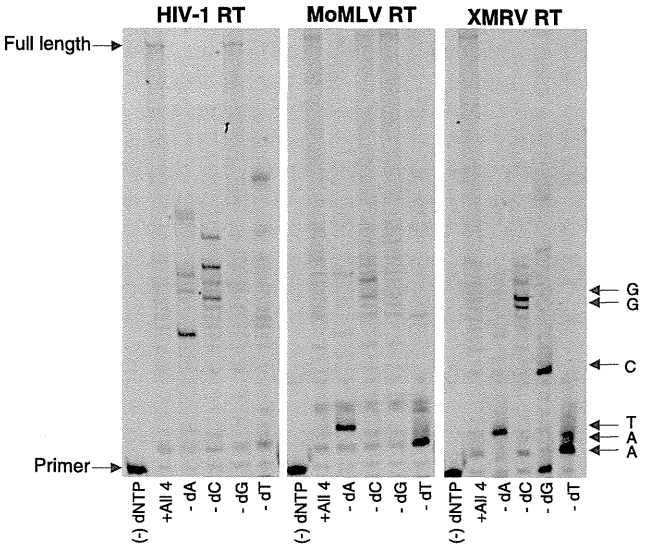

Figure 3. Comparison of *in vitro* fidelity of HIV-1, MoMLV and XMRV RTs. Extension of 10 nM T_{d100}/5′-Cy3-P_{d18a} by HIV-1 RT, MoMLV RT or XMRV RT (20, 50 and 50 nM, respectively) in the presence of 150 μM each of three out of four nucleotides (the missing nucleotide is marked at the bottom of each lane). Reactions were run for 30 min for HIV-1 RT and 45 min for XMRV RT and MoMLV RT. For each enzyme the first lane in each set shows the position of unextended primer, the second lane shows full extension in the presence of all four dNTPs, and each consecutive lane shows extension in the presence of three dNTPs. The arrows on the right mark the expected pauses based on the indicated composition of the template strand.

Table 4. Kinetics of mismatch incorporation for HIV-1, MoMLV and XMRV RTs

Enzyme	HIV-1 RT	MoMLV RT	XMRV RT
$K_{d.dNTP}$ (μM)	9 ± 0.3	38.9 ± 11.6	256 ± 72
k_{pol} (s^{-1})	6.81 ± 1.2	0.16 ± 0.01	0.15 ± 0.018
$k_{pol}/K_{d.dNTP}$ (s^{-1} • μM)	0.756	0.0041	0.00058
Fidelity[a]	0.04	0.007	0.002

[a]Fidelity is the ratio of the incorporation efficiency ($k_{pol}/K_{d.dNTP}$) of the mismatched nucleotide (dTTP) over that of the correct (dATP) ([k_{pol}/K_d]dTTP/[k_{pol}/K_d]dATP).

Intracellular fidelity by measuring LacZ mutation frequency

The ANGIE P cells used for this assay are a D17-based encapsidating cell line and contain an MLV-based retroviral vector (GA-1), which encodes a bacterial β-galactosidase gene (*lacZ*) and a neomycin phosphotransferase gene (*neo*). Replication fidelity is a measure of the frequency of *lacZ* inactivation and was determined by measuring *lacZ* non-expressing white colonies. The results show that the number of white colonies was not statistically different in the case of XMRV as compared to AM-MLV, suggesting that under these conditions the fidelity of XMRV is not significantly different than that of AM-MLV (Figure 4).

Processivity of DNA synthesis

Processivity is the probability of translocation of a polymerase along a template and predicts the number of cycles of nucleotide incorporation during one productive enzyme–DNA binding event. We assessed XMRV RT's processivity of DNA synthesis in comparison to HIV and MoMLV RTs using both a gel-based trap assay and a quantitative pre-steady state assay. In the gel-based assay, the enzymes were pre-incubated with template-primer, then the reaction was initiated by the addition of all four nucleotides together with calf thymus DNA, which was used as a trap to bind free enzyme dissociated from the substrate during the course of the reaction (38). The length of the DNA product is an inverse measure of termination probability, as previously described. As a control, we used lanes where no trap was present; establishing that the same amount of total polymerase activity (processive and non-processive) is provided in all cases. The results indicate that XMRV RT is less processive than HIV-1 and MoMLV RTs with shorter DNA product after 30 min of reaction in the presence of trap (Figure 5).

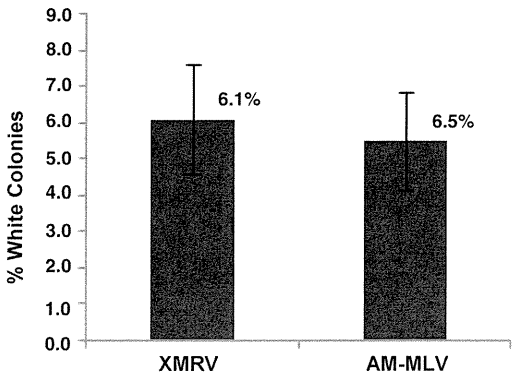

Figure 4. Comparison of *in vivo* fidelity of XMRV with amphotropic MLV. The ANGIE P cells used for this assay contain a retroviral vector (GA-1), which encodes a bacterial β-galactosidase gene (*lacZ*) and a neomycin phosphotransferase gene. Replication fidelity is measured by the frequency of *lacZ* inactivation resulting in an increase in white colonies. The fidelity differences between the two viruses are not statistically significant (error bars represent standard error from three independent experiments).

To measure processivity quantitatively we applied a single turnover processivity assay developed by Patel *et al.* (35) (Figure 6). In this assay, the rates of consecutive nucleotide incorporations under single turnover conditions are monitored. The rate of elongation incorporation (k_1) and the rate of processive DNA synthesis (k_2) (Equation 4) were calculated at several template positions for each enzyme. The ratio of the rate of processive DNA synthesis to the rate of nucleotide incorporation (k_2/k_1) is referred to as the processivity index (35). The absolute values of these constants for HIV-1 RT, XMRV and MoMLV RT and their ratios are collected in Table 5. XMRV RT is clearly the least processive for each extension product. The difference in processivity varies significantly depending on sequence or sequence context (decrease in processivity from 3-fold up to 10-fold). While the current data do not allow generalization of rules for pausing at specific sites, this clearly shows consistently that XMRV is not as efficient as MoMLV RT in polymerizing processively through 'difficult spots'.

Susceptibility of XMRV RT to NRTIs, TDRTIs and NNRTIs

Previous studies have shown that XMRV is inhibited by some antivirals (53–56). However, the susceptibility of XMRV RT has not been tested against a wide variety of

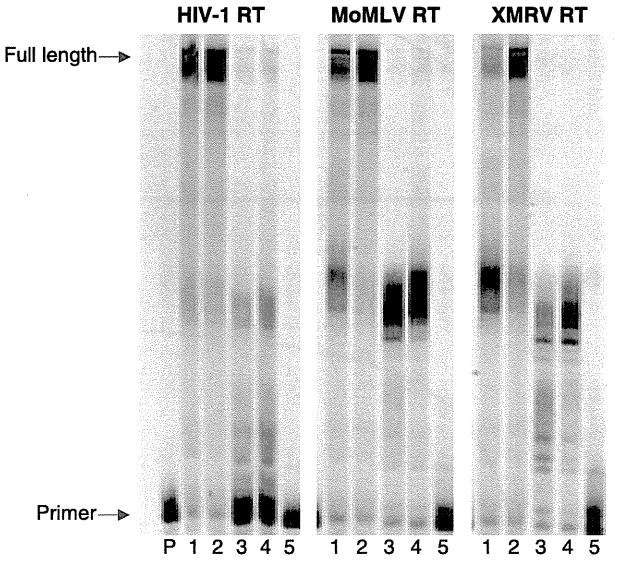

Figure 5. Processivity (trap assay) of HIV-RT, MoMLV RT and XMRV RT. DNA synthesis was monitored in the presence of calf thymus DNA as an enzyme trap. Each enzyme (30 nM HIV RT, 100 nM MoMLV RT or 100 nM XMRV RT) was pre-incubated with 40 nM T_{d100}/Cy3-P_{d18a}. Lanes 1 and 2 of each set show unlimited DNA synthesis in the absence of trap for 5 and 10 min for HIV-1 RT and 10 and 40 min for XMRV RT and MoMLV RT. In Lanes 3 and 4 the reaction is initiated by the addition of dNTPs (100 μM each) together with the calf thymus DNA trap (0.5 μg/μl) such that the products generated represent a single processive synthesis event for the respective time points for each enzyme. Lane 5 shows the effectiveness of the trap determined by incubating the calf thymus DNA with the enzyme before addition of labeled template-primer. Processive primer extension by HIV-1 RT and MoMLV RT in Lanes 4–6 of the left and middle panel is higher than by XMRV RT in Lanes 4–6 of the right panel.

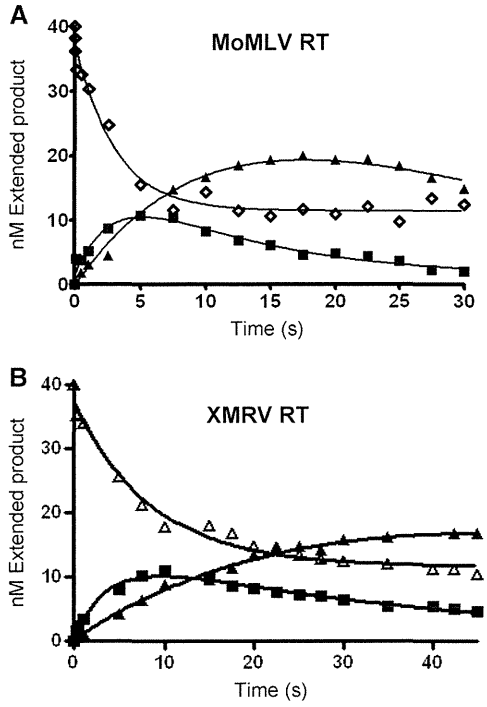

Figure 6. Single-turnover processivity assays. 30 nM T_{d31}/Cy3-P_{d18a} was combined with 100 nM XMRV RT or 50 nM MoMLV RT in RT buffer before rapidly mixing with all four dNTPs (100 μM each) and 5 mM $MgCl_2$ for varying incubation times (0.05–45 s) and quenching with EDTA. Extension of the 18-mer primer (open rhombus) ((open triangle) for XMRV RT) into 19-mer (filled square) and 22-mer (filled square), by MoMLV RT (**A**) and XMRV RT (**B**) was fit to a double exponential equation to determine rates of product appearance, and subsequent processive extension of those products (rates shown in Table 5).

Table 5. Single turnover processivity parameters of HIV-1, MoMLV and XMRV RTs

Template site	Processivity index (k_2/k_1)		
	HIV-1 RT	MoMLV RT	XMRV RT
1	6.98	0.31	0.12

1
3′-CAT TGA CAA GCT CGT GGT TAC GAT CGA TAC C
5′-Cy3-GTA ACT GTT CGA GCA CCT
The template site position monitored is underlined and labeled.

nucleoside RT inhibitors (NRTIs) that block replication by chain-terminating the primer, or by preventing translocation after their incorporation into the nascent DNA chain (TDRTIs) (32,57,58). In addition, the susceptibility of XMRV RT to non-nucleoside RT inhibitors (NNRTIs) or RNA aptamers that can be selected to block reverse transcriptases (59–63) has not been established.

Hence, we performed gel-based primer extension assays in the presence of various inhibitors. As shown in Table 6, most of the HIV-1 RT inhibitors also block XMRV RT with significantly varying IC_{50}s. The most potent inhibitors tested were ENdA (4′-ethynyl-2-amino-2′-deoxyadenosine) followed by EFdA. EFdA was also potent at

Table 6. Inhibition of XMRV and MoMLV RTs

Compound	IC_{50} (μM)	
	XMRV RT	MoMLV RT
Adefovir-DP	0.92	1.02
Tenofovir-DP	6.4	1.51
D4T-TP	0.77	2.37
3TC-TP	21	10
EFdA-TP	0.43	0.29
ENdA-TP	0.14	0.18

D4T, stavudine or 2′,3′-dehydro-2′,3′-deoxythymidine; 3TC, lamivudine; EFdA, 4′-ethynyl-2-fluoro-2′-deoxyadenosine; ENdA, 4′-ethynyl-2-amino-2′-deoxyadenosine.

inhibiting wild-type XMRV replication in cell culture with an EC_{50} of 40 nM from three independent experiments (standard error was 10 nM).

Unlike HIV-1 RT, XMRV RT and MoMLV RT lack the two tyrosine residues (Y181 andY188 in HIV-1 RT) (Supplementary Figure S1) that are known to contribute to NNRTI binding. Hence, the gammaretroviral enzymes were not inhibited by the NNRTIs tested (TMC-125 and efavirenz) (Supplementary Figure S3).

Susceptibility of XMRV RT to RNA aptamers

We also tested XMRV RT's susceptibility to three independent RNA aptamers that had been previously selected against MoMLV RT (60). The aptamers inhibited XMRV RT to varying extents with IC_{50}s ranging from 2 to 52 nM (Figure 7). Most notable was the m.1.1FL aptamer which gave IC_{50}s of 2 and 4 nM for XMRV RT (Figure 7) and MoMLV RT respectively, without inhibiting HIV-1 RT (data not shown). These inhibition assays utilized truncated forms of aptamers m.1.3 and m.1.4 lacking the original primer-binding segments of the aptamers, demonstrating that these 5′ and 3′ segments are not required.

PPi-mediated excision activity of XMRV RT

A key mechanism of NRTI resistance in HIV-1 RT is based on inhibitor excision from the primer end, using a pyrophospholytic reaction (64,65). The pyrophosphate donor *in vivo* is likely to be ATP, although PPi can efficiently unblock NRTI-terminated primers. This excision activity is present in wild-type HIV-1 RT, and is enhanced in the presence of AZT-resistance mutations. We measured the ability of wild-type XMRV to unblock primers terminated with AZT or EFdA in the presence of PPi. We found that unlike HIV-1 RT that excised AZT-MP efficiently under these conditions, XMRV RT had considerably lower excision activity (Figure 8). Similar excision experiments where ATP was used instead of PPi showed that XMRV is very inefficient in ATP-based excision as compared to HIV-1 RT (data not shown).

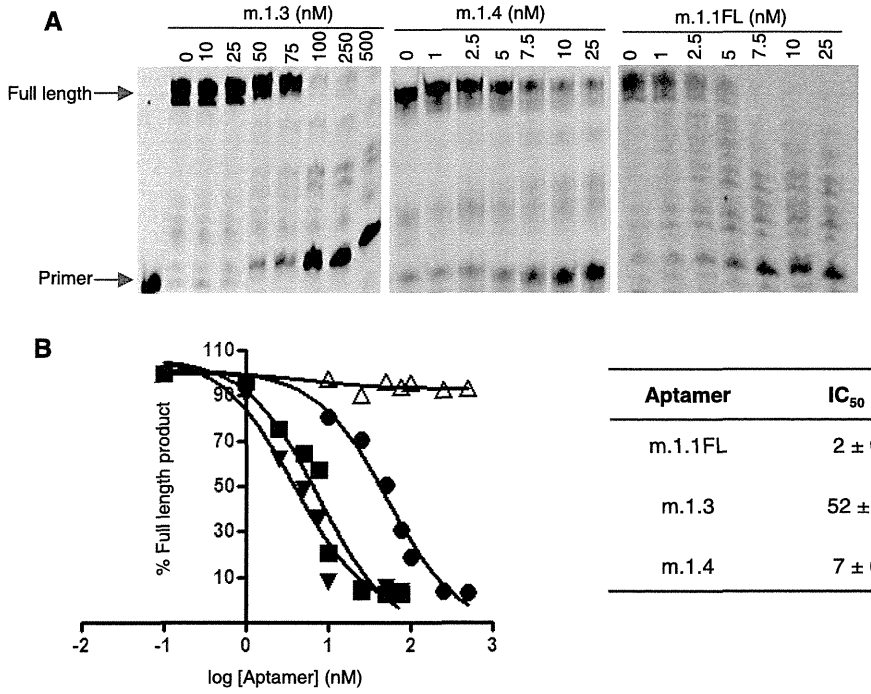

Aptamer	IC_{50} (nM)
m.1.1FL	2 ± 0.15
m.1.3	52 ± 0.27
m.1.4	7 ± 0.16

Figure 7. Inhibition of XMRV RT by RNA aptamers. 10 nM XMRV RT was incubated with increasing amounts of RNA aptamer in Reaction Buffer for 5 min at 37°C followed by addition of 20 nM T_{d31}/Cy3-P_{d18a} and 50 μM of each dNTP. (**A**) The reactions were stopped after 30 min and resolved on a polyacrylamide gel. The predicted secondary structures of each aptamer were generated by mfold. (**B**) The percent full extension was quantified for m.1.1FL (filled inverted triangle), m.1.3 (filled circle) and m.1.4 (filled square) and data points fit to one-site competition non-linear regression using GraphPad Prism 4 to calculate IC_{50}. HIV-1 RT was not susceptible to m.1.1FL (open triangle). (Errors represent data deviation from the fit).

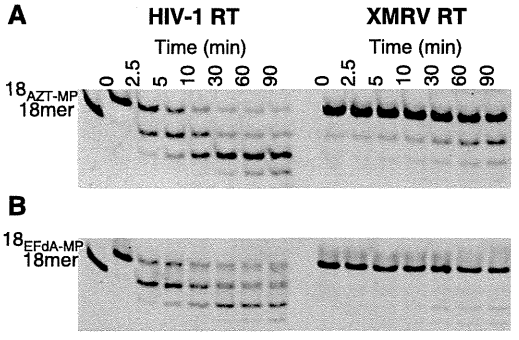

Figure 8. PPi-mediated unblocking of AZT-(A) and EFdA-(B) terminated DNA. About 20 nM of (**A**) AZT- or (**B**) EFdA-terminated T_{d31}/Cy3-P_{d18c} ($T/P_{AZT\text{-}MP}$ or $T/P_{EFdA\text{-}MP}$) was incubated with HIV-1 RT (60 nM) or XMRV RT (200 nM) in the presence of 150 μM PPi and 6 mM $MgCl_2$. Aliquots of the reactions were stopped at different time points (0–90 min) and resolved on a 15% polyacrylamide–7M urea gel as described in the 'Materials and Methods' section.

Susceptibility of mutant XMRV RTs to AZT-TP and tenofovir-DP

The HIV-1 RT mutation Q151M confers resistance to AZT by enhancing discrimination of the nucleotide analog leading to its reduced incorporation (37,66–68). Another HIV-1 RT mutation, K65R, decreases susceptibility to tenofovir (69,70). Since AZT and tenofovir are potent inhibitors of XMRV (Table 6) (54–56), we wanted to investigate whether the XMRV RT mutant equivalents of HIV Q151M and K65R (XMRV Q190M and K103R) would confer XMRV RT resistance to AZT and tenofovir. We constructed these mutant clones and tested their susceptibility to AZT and tenofovir in the same manner as wild-type XMRV RT. Interestingly, Q190M XMRV RT has a decreased susceptibility to AZT (approximately 5-fold increase in the IC_{50}). Similarly, the K103R XMRV RT mutant enzyme was less susceptible to tenofovir, increasing the IC_{50} by at least 2-fold.

Molecular model of XMRV RT

Given the significant sequence similarity between XMRV and MoMLV RTs, the resulting homology model of XMRV RT is highly similar to MoMLV RT (>1.5Å rms) and of excellent quality. Since the input structure of MoMLV RT did not contain the RNase H domain of the enzyme, the XMRV RT model is also missing this domain. The molecular model of the polymerase domain of XMRV RT is shown in Figure 9. An alignment of the MoMLV RT crystal structure (22) with the XMRV RT homology model highlights the few changes in the polymerase domain of XMRV RT. These are L29 (P in MoMLV), Q234 (L in MoMLV), R238 (Q in MoMLV) and N422 (D in MoMLV). From these, residue 422 is located in the nucleic acid binding cleft and may contribute to differences in the interactions with nucleic acid substrate. However, most of the differences between the gammaretroviral enzymes are in their RNase H domains and also in the first 30 N-terminal residues of the polymerase domain, for which we do not have structural

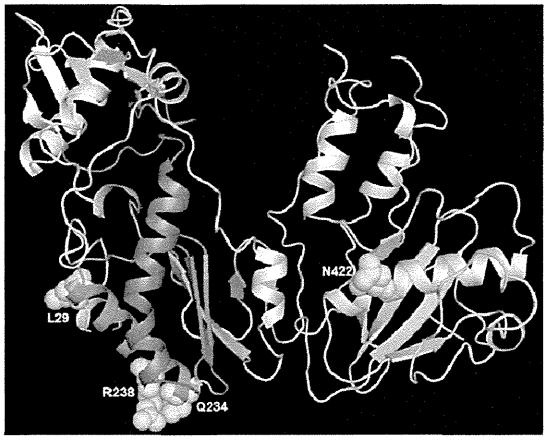

Figure 9. Molecular model of XMRV RT. Ribbons diagram of XMRV RT with the conserved polymerase Motifs color-coded: Motif A (green), B (brown), C (purple), D (red), E (orange) and F (blue). The residues that differ from MoMLV's polymerase domain are shown in ball and stick representation.

information since they were not included in the original crystal structure of MoMLV RT. The differences between XMRV RT and HIV-1 RT are very significant. Unlike the HIV enzyme, XMRV RT appears to be a monomer in solution. Moreover, alignment of the HIV-1 RT–DNA complex with XMRV RT based on their active sites at the palm subdomains shows that the thumb subdomain of XMRV RT would have to be repositioned to be able to accommodate nucleic acid.

DISCUSSION

Early studies reported the presence of XMRV in stromal cells from prostate cancer patient samples and also in CFS clinical samples. Some of the subsequent studies confirmed these findings whereas several others failed to identify XMRV in prostate cancer or in CFS patients, even when same samples were used (71). It was recently reported that human sample contamination with mouse DNA can occur frequently (17,72–74). Moreover, two coauthors from this study have recently demonstrated that XMRV is the product of recombination events between two MLV proviruses, suggesting that XMRV may not be relevant to human disease (18). Nonetheless, XMRV is still an important human retrovirus and comparisons with HIV can provide valuable insights into the fundamental mechanisms of DNA polymerization, RT inhibition and drug resistance. (75).

There is high degree of sequence similarity between the XMRV and MoMLV RTs (95% amino acid identity), and much less so with HIV-1 RT. Based on gel filtration experiments we conclude that unlike HIV-1 RT, but similar to MoMLV RT, XMRV RT exists in solution primarily as a monomer. We also included comparisons with HIV-1 RT in this study as it has been extensively studied and provides an excellent frame of reference.

We report here that there are significant differences in the DNA polymerization efficiency of the three enzymes. Although the polymerase active sites of the XMRV and MoMLV enzymes are almost identical, there is a considerable decrease in the efficiency of nucleotide incorporation by XMRV RT. Most differences in sequence are at the RNase H domain and are likely to affect polymerization by changing the positioning of DNA at the polymerase active site.

We have recently solved the crystal structure of the XMRV RNase H at high resolution (1.5Å) (pdb 3P1G) (Kirby, K.A. *et al.*, submitted for publication). We observed major differences in affinity for nucleic acid that we determined with gel-mobility shift assays and with pre-steady state kinetics. SPR experiments dissected in more detail the specific defect of XMRV RT in binding DNA. Surprisingly, XMRV RT can associate very rapidly with DNA, even more so than HIV-1 RT (Figure 1 and Table 3). However, it dissociates from DNA much faster than the HIV enzyme, resulting in an overall reduced binding affinity. A possible reason for the fast association and dissociation rates of XMRV RT may be the apparent monomeric state, which might offer facile access to the nucleic acid binding cleft, although with less contacts and lower affinity than HIV-1 RT, which is a heterodimer (76,77). This high rate of XMRV RT dissociation from DNA likely contributes to the decreased processivity observed in our study, and may have consequences in the recombination rates of this virus.

Previous sequences of XMRV from prostate cancer tumors showed low variability, suggesting that the virus may have a high fidelity of replication (1,10). Our study demonstrated that HIV-1 RT and MoMLV RT incorporated mismatched nucleotides and extended past the mismatches more efficiently than XMRV RT. Pre-steady state kinetics established that the higher overall fidelity of XMRV RT over MoMLV RT is due to a lower affinity for mismatched nucleotides. When compared to HIV-1 RT, however, XMRV RT has differs in both the nucleotide binding and incorporation steps. Nonetheless, XMRV did not have higher fidelity than a related amphotropic MLV virus or HIV-1 in a cell-based assay. It is possible that the high dNTP concentration in dividing cells can suppress mismatching events. We have previously shown (39) that as nucleotide concentrations vary in different cell lines, this can affect viral susceptibility to NRTIs, and possibly in this case also incorporation of mismatched nucleotides. Additional cell-based studies using multiple cell lines and a large panel of viruses should provide a better understanding of the relation between *in vivo* and *in vitro* fidelity.

Early studies have reported susceptibility of XMRV to some antiretrovirals that have been used in the treatment of HIV infection (53–56). In those studies the compounds were tested at the virus level. To better understand the interactions of inhibitors at their RT target level we tested here the ability of these and several more compounds to block the polymerase activity of XMRV RT. We found that two TDRTIs, EFdA-TP and ENdA-TP were very potent RT inhibitors (IC_{50}s: 0.43 μM and 0.14 μM, respectively). Unlike other NRTIs, these compounds have a 3′ OH group and are known to efficiently inhibit HIV replication by blocking translocation (32,58,78).

Preliminary experiments demonstrated that they also block XMRV RT by the same mechanism (data not shown).

In HIV, moderate resistance to EFdA is conferred by the emergence of the M184V mutation at the conserved X position of the conserved YXDD motif of the polymerase active site. Interestingly, XMRV and MoMLV RTs already have a valine (V223) at this position. This difference is likely to contribute to the better potency of EFdA against HIV-1 RT than XMRV RT or MoMLV RT (57,58). It may also contribute to the decreased ability of XMRV RT to unblock chain-terminated primers, as was also reported for M184V HIV-1 RT (79) and to the enhanced fidelity reported here for XMRV RT, which is also reminiscent of the previously reported high fidelity of M184V HIV-1 RT (80,81). Nonetheless, despite the presence of a Val in the YMDD motif of XMRV RT we found EFdA to inhibit very efficiently replication-competent or pseudotyped XMRV, with submicromolar EC_{50}s (40 and 110 nM, respectively).

Previously, highly potent aptamers were selected to inhibit MoMLV RT (60). We demonstrate here that the three aptamers we tested have varying potency against XMRV RT. Aptamer m.1.1FL was the most potent inhibitor of XMRV RT and MoMLV RT in *in vitro* assays (IC_{50} = 2 and 4 nM, respectively). The fact that XMRV and MoMLV RTs are inhibited by the same aptamers at comparable efficiencies suggests that the RT residues that are different in the two enzymes are not critical to the binding of the aptamer. In contrast, heterodimeric HIV-1 RT has a very different binding cleft and is not inhibited by these aptamers.

Tenofovir is an essential component of HIV therapies and is also a potent inhibitor of XMRV RT. HIV resistance to tenofovir is conferred by a single codon mutation (K65R). HIV-1 RT residue 65 is known to interact with the incoming dNTP or the activated tenofovir analog (tenofovir diphosphate) (82). K65R causes resistance to tenofovir by lowering the k_{pol} for the incorporation of the inhibitor into the nascent DNA. We prepared XMRV RT with the equivalent mutation, K103R, and determined that it has decreased susceptibility to tenofovir. Hence, it is possible for XMRV to develop tenofovir resistance through the same mechanism as HIV-1 RT. HIV resistance to AZT can occur by either decreased binding/incorporation or increased excision of the chain-terminating NRTI (33,83). HIV-1 RTs containing the M41L, D67N, K70R, T215Y/F, K219E/Q mutations show enhanced removal of AZT. Our experiments show that unlike wild-type HIV-1 RT, XMRV RT is not able to excise NRTI-terminated primers. Similarly, it was previously shown that MoMLV RT is not capable of unblocking chain-terminated primers (33).

In HIV, decreased binding of AZT is conferred initially in the presence of the primary Q151M mutation, followed by secondary mutations F77L, A62V, V75I and F116Y (27,47,84). XMRV RT already differs from wild-type HIV-1 RT in the first three of these residues (P104, Q113 and L115 versus A62, V75 and F77) (Table 1). We demonstrated that introducing the primary Q→M mutation at the equivalent XMRV RT site (Q190M) resulted in an enzyme with decreased susceptibility to AZT. Hence, it appears that these residues can confer AZT resistance to XMRV by reduced incorporation of nucleotide analogs, as is the case in HIV-2 (41). At this point we do not know if introduction of as yet unknown mutations could endow XMRV RT with the ability to unblock chain-terminated nucleic acids. The details of the molecular mechanism of XMRV resistance to tenofovir and AZT are under investigation.

In conclusion, our study provides detailed biochemical analysis of the mechanisms of polymerization, inhibition, fidelity, processivity and drug resistance of XMRV RT and how it compares with the closely related enzyme MoMLV RT and the more distantly related HIV-1 RT. The findings enhance our understanding of the basic mechanisms of reverse transcription.

SUPPLEMENTARY DATA

Supplementary Data are available at NAR Online.

ACKNOWLEDGEMENTS

The content of this publication does not necessarily reflect the views or policies of the Department of Health Human Services, nor does mention of trade names, commercial products or organizations imply endorsement by the U.S. Government.

FUNDING

NIH grants (AI076119, AI079801, and AI094715, to S.G.S.), (AI074389, to D.H.B.), (AI079801 to M.A.P.); NIH Bench-to-Bedside Award and the Intramural Research Program of the NIH, National Cancer Institute, Center for Cancer Research (to V.K.P); Ministry of Knowledge and Economy, Bilateral International Collaborative R&D Program, Republic of Korea; Canadian Institutes of Health Research (CIHR) and University of Missouri (to S-L.L.); amfAR Mathilde Krim Fellowship and a CIHR Fellowship (to B.M.). Funding for open access charge: NIH grants (AI076119, AI094715, AI074389, AI079801).

Conflict of interest statement. None declared.

REFERENCES

1. Urisman,A., Molinaro,R.J., Fischer,N., Plummer,S.J., Casey,G., Klein,E.A., Malathi,K., Magi-Galluzzi,C., Tubbs,R.R., Ganem,D. *et al.* (2006) Identification of a novel gammaretrovirus in prostate tumors of patients homozygous for R462Q RNASEL variant. *PLoS Pathog.*, **2**, e25.
2. Malathi,K., Dong,B., Gale,M. Jr. and Silverman,R.H. (2007) Small self-RNA generated by RNase L amplifies antiviral innate immunity. *Nature*, **448**, 816–819.
3. Arnold,R.S., Makarova,N.V., Osunkoya,A.O., Suppiah,S., Scott,T.A., Johnson,N.A., Bhosle,S.M., Liotta,D., Hunter,E., Marshall,F.F. *et al.* XMRV infection in patients with prostate cancer: novel serologic assay and correlation with PCR and FISH. *Urology*, **75**, 755–761.
4. Dong,B., Kim,S., Hong,S., Das Gupta,J., Malathi,K., Klein,E.A., Ganem,D., Derisi,J.L., Chow,S.A. and Silverman,R.H. (2007) An

infectious retrovirus susceptible to an IFN antiviral pathway from human prostate tumors. *Proc Natl Acad Sci. USA*, **104**, 1655–1660.
5. Knouf,E.C., Metzger,M.J., Mitchell,P.S., Arroyo,J.D., Chevillet,J.R., Tewari,M. and Miller,A.D. (2009) Multiple integrated copies and high-level production of the human retrovirus XMRV (xenotropic murine leukemia virus-related virus) from 22Rv1 prostate carcinoma cells. *J. Virol.*, **83**, 7353–7356.
6. Schlaberg,R., Choe,D.J., Brown,K.R., Thaker,H.M. and Singh,I.R. (2009) XMRV is present in malignant prostatic epithelium and is associated with prostate cancer, especially high-grade tumors. *Proc. Natl Acad. Sci. USA*, **106**, 16351–16356.
7. Sabunciyan,S., Mandelberg,N., Rabkin,C.S., Yolken,R. and Viscidi,R. No difference in antibody titers against xenotropic MLV related virus in prostate cancer cases and cancer-free controls. *Mol. Cell. Probes.*, **25**, 134–136.
8. Verhaegh,G.W., de Jong,A.S., Smit,F.P., Jannink,S.A., Melchers,W.J. and Schalken,J.A. (2011) Prevalence of human xenotropic murine leukemia virus-related gammaretrovirus (XMRV) in Dutch prostate cancer patients. *Prostate*, **71**, 415–420.
9. Hohn,O., Krause,H., Barbarotto,P., Niederstadt,L., Beimforde,N., Denner,J., Miller,K., Kurth,R. and Bannert,N. (2009) Lack of evidence for xenotropic murine leukemia virus-related virus(XMRV) in German prostate cancer patients. *Retrovirology*, **6**, 92.
10. Lombardi,V.C., Ruscetti,F.W., Das Gupta,J., Pfost,M.A., Hagen,K.S., Peterson,D.L., Ruscetti,S.K., Bagni,R.K., Petrow-Sadowski,C., Gold,B. *et al.* (2009) Detection of an infectious retrovirus, XMRV, in blood cells of patients with chronic fatigue syndrome. *Science*, **326**, 585–589.
11. Henrich,T.J., Li,J.Z., Felsenstein,D., Kotton,C.N., Plenge,R.M., Pereyra,F., Marty,F.M., Lin,N.H., Grazioso,P., Crochiere,D.M. *et al.* (2010) Xenotropic murine leukemia virus-related virus prevalence in patients with chronic fatigue syndrome or chronic immunomodulatory conditions. *J. Infect. Dis.*, **202**, 1478–1481.
12. Erlwein,O., Kaye,S., McClure,M.O., Weber,J., Wills,G., Collier,D., Wessely,S. and Cleare,A. (2010) Failure to detect the novel retrovirus XMRV in chronic fatigue syndrome. *PLoS ONE*, **5**, e8519.
13. Groom,H.C., Boucherit,V.C., Makinson,K., Randal,E., Baptista,S., Hagan,S., Gow,J.W., Mattes,F.M., Breuer,J., Kerr,J.R. *et al.* (2010) Absence of xenotropic murine leukaemia virus-related virus in UK patients with chronic fatigue syndrome. *Retrovirology*, **7**, 10.
14. Switzer,W.M., Jia,H., Hohn,O., Zheng,H., Tang,S., Shankar,A., Bannert,N., Simmons,G., Hendry,R.M., Falkenberg,V.R. *et al.* (2010) Absence of evidence of xenotropic murine leukemia virus-related virus infection in persons with chronic fatigue syndrome and healthy controls in the United States. *Retrovirology*, **7**, 57.
15. Satterfield,B.C., Garcia,R.A., Jia,H., Tang,S., Zheng,H. and Switzer,W.M. (2011) Serologic and PCR testing of persons with chronic fatigue syndrome in the United States shows no association with xenotropic or polytropic murine leukemia virus-related viruses. *Retrovirology*, **8**, 12.
16. Menendez-Arias,L. Evidence and controversies on the role of XMRV in prostate cancer and chronic fatigue syndrome. *Rev. Med. Virol.*, **21**, 3–17.
17. Hue,S., Gray,E.R., Gall,A., Katzourakis,A., Tan,C.P., Houldcroft,C.J., McLaren,S., Pillay,D., Futreal,A., Garson,J.A. *et al.* (2010) Disease-associated XMRV sequences are consistent with laboratory contamination. *Retrovirology*, **7**, 111.
18. Paprotka,T., Delviks-Frankenberry,K.A., Cingoz,O., Martinez,A., Kung,H.J., Tepper,C.G., Hu,W.S., Fivash,M.J. Jr., Coffin,J.M. and Pathak,V.K. (2011) Recombinant origin of the retrovirus XMRV. *Science*, **333**, 97–101.
19. Singh,K., Kaushik,N., Jin,J., Madhusudanan,M. and Modak,M.J. (2000) Role of Q190 of MuLV RT in ddNTP resistance and fidelity of DNA synthesis: a molecular model of interactions with substrates. *Protein Eng.*, **13**, 635–643.
20. Telesnitsky,A. and Goff,S.P. (1993) Two defective forms of reverse transcriptase can complement to restore retroviral infectivity. *EMBO J.*, **12**, 4433–4438.
21. Georgiadis,M.M., Jessen,S.M., Ogata,C.M., Telesnitsky,A., Goff,S.P. and Hendrickson,W.A. (1995) Mechanistic implications from the structure of a catalytic fragment of Moloney murine leukemia virus reverse transcriptase. *Structure*, **3**, 879–892.
22. Das,D. and Georgiadis,M.M. (2004) The crystal structure of the monomeric reverse transcriptase from Moloney murine leukemia virus. *Structure*, **12**, 819–829.
23. Chowdhury,K., Kaushik,N., Pandey,V.N. and Modak,M.J. (1996) Elucidation of the role of Arg 110 of murine leukemia virus reverse transcriptase in the catalytic mechanism: biochemical characterization of its mutant enzymes. *Biochemistry*, **35**, 16610–16620.
24. Kaushik,N., Chowdhury,K., Pandey,V.N. and Modak,M.J. (2000) Valine of the YVDD motif of moloney murine leukemia virus reverse transcriptase: role in the fidelity of DNA synthesis. *Biochemistry*, **39**, 5155–5165.
25. Jacobo-Molina,A., Ding,J., Nanni,R.G., Clark,A.D. Jr., Lu,X., Tantillo,C., Williams,R.L., Kamer,G., Ferris,A.L., Clark,P. *et al.* (1993) Crystal structure of human immunodeficiency virus type 1 reverse transcriptase complexed with double-stranded DNA at 3.0 A resolution shows bent DNA. *Proc. Natl Acad. Sci. USA*, **90**, 6320–6324.
26. Kohlstaedt,L.A., Wang,J., Friedman,J.M., Rice,P.A. and Steitz,T.A. (1992) Crystal structure at 3.5 A resolution of HIV-1 reverse transcriptase complexed with an inhibitor. *Science*, **256**, 1783–1790.
27. Sarafianos,S.G., Marchand,B., Das,K., Himmel,D.M., Parniak,M.A., Hughes,S.H. and Arnold,E. (2009) Structure and function of HIV-1 reverse transcriptase: molecular mechanisms of polymerization and inhibition. *J. Mol. Biol.*, **385**, 693–713.
28. Singh,K., Marchand,B., Kirby,K.A., Michailidis,E. and Sarafianos,S.G. (2010) Structural aspects of drug resistance and inhibition of HIV-1 reverse transcriptase. *Viruses*, **2**, 606–638.
29. Schuckmann,M.M., Marchand,B., Hachiya,A., Kodama,E.N., Kirby,K.A., Singh,K. and Sarafianos,S.G. (2010) The N348I mutation at the connection subdomain of HIV-1 reverse transcriptase decreases binding to nevirapine. *J. Biol. Chem.*, **285**, 38700–38709.
30. Telesnitsky,A. and Goff,S.P. (1993) RNase H domain mutations affect the interaction between Moloney murine leukemia virus reverse transcriptase and its primer-template. *Proc. Natl Acad. Sci. USA*, **90**, 1276–1280.
31. Bauman,J.D., Das,K., Ho,W.C., Baweja,M., Himmel,D.M., Clark,A.D. Jr., Oren,D.A., Boyer,P.L., Hughes,S.H., Shatkin,A.J. *et al.* (2008) Crystal engineering of HIV-1 reverse transcriptase for structure-based drug design. *Nucleic Acids Res.*, **36**, 5083–5092.
32. Michailidis,E., Marchand,B., Kodama,E.N., Singh,K., Matsuoka,M., Kirby,K.A., Ryan,E.M., Sawani,A.M., Nagy,E., Ashida,N. *et al.* (2009) Mechanism of inhibition of HIV-1 reverse transcriptase by 4′-Ethynyl-2-fluoro-2′-deoxyadenosine triphosphate, a translocation-defective reverse transcriptase inhibitor. *J. Biol. Chem.*, **284**, 35681–35691.
33. Meyer,P.R., Matsuura,S.E., So,A.G. and Scott,W.A. (1998) Unblocking of chain-terminated primer by HIV-1 reverse transcriptase through a nucleotide-dependent mechanism. *Proc. Natl Acad. Sci. USA*, **95**, 13471–13476.
34. Halvas,E.K., Svarovskaia,E.S. and Pathak,V.K. (2000) Development of an in vivo assay to identify structural determinants in murine leukemia virus reverse transcriptase important for fidelity. *J Virol*, **74**, 312–319.
35. Patel,S.S., Wong,I. and Johnson,K.A. (1991) Pre-steady-state kinetic analysis of processive DNA replication including complete characterization of an exonuclease-deficient mutant. *Biochemistry*, **30**, 511–525.
36. Sarafianos,S.G., Clark,A.D. Jr., Das,K., Tuske,S., Birktoft,J.J., Ilankumaran,P., Ramesha,A.R., Sayer,J.M., Jerina,D.M., Boyer,P.L. *et al.* (2002) Structures of HIV-1 reverse transcriptase with pre- and post-translocation AZTMP-terminated DNA. *EMBO J.*, **21**, 6614–6624.
37. Tuske,S., Sarafianos,S.G., Clark,A.D. Jr., Ding,J., Naeger,L.K., White,K.L., Miller,M.D., Gibbs,C.S., Boyer,P.L., Clark,P. *et al.* (2004) Structures of HIV-1 RT-DNA complexes before and after

incorporation of the anti-AIDS drug tenofovir. *Nat. Struct. Mol. Biol.*, **11**, 469–474.
38. Sarafianos,S.G., Pandey,V.N., Kaushik,N. and Modak,M.J. (1995) Site-directed mutagenesis of arginine 72 of HIV-1 reverse transcriptase. Catalytic role and inhibitor sensitivity. *J. Biol. Chem.*, **270**, 19729–19735.
39. Hachiya,A., Kodama,E.N., Schuckmann,M.M., Kirby,K.A., Michailidis,E., Sakagami,Y., Oka,S., Singh,K. and Sarafianos,S.G. (2011) K70Q adds high-level tenofovir resistance to "Q151M complex" HIV reverse transcriptase through the enhanced discrimination mechanism. *PLoS One*, **6**, e16242.
40. Sarafianos,S.G., Das,K., Ding,J., Boyer,P.L., Hughes,S.H. and Arnold,E. (1999) Touching the heart of HIV-1 drug resistance: the fingers close down on the dNTP at the polymerase active site. *Chem. Biol.*, **6**, R137–R146.
41. Boyer,P.L., Sarafianos,S.G., Clark,P.K., Arnold,E. and Hughes,S.H. (2006) Why do HIV-1 and HIV-2 use different pathways to develop AZT resistance? *PLoS Pathog.*, **2**, e10.
42. Powell,M.D., Ghosh,M., Jacques,P.S., Howard,K.J., Le Grice,S.F. and Levin,J.G. (1997) Alanine-scanning mutations in the "primer grip" of p66 HIV-1 reverse transcriptase result in selective loss of RNA priming activity. *J. Biol. Chem.*, **272**, 13262–13269.
43. Sarafianos,S.G., Das,K., Clark,A.D. Jr., Ding,J., Boyer,P.L., Hughes,S.H. and Arnold,E. (1999) Lamivudine (3TC) resistance in HIV-1 reverse transcriptase involves steric hindrance with beta-branched amino acids. *Proc. Natl Acad. Sci. USA*, **96**, 10027–10032.
44. Boucher,C.A., Cammack,N., Schipper,P., Schuurman,R., Rouse,P., Wainberg,M.A. and Cameron,J.M. (1993) High-level resistance to (-) enantiomeric 2′-deoxy-3′-thiacytidine in vitro is due to one amino acid substitution in the catalytic site of human immunodeficiency virus type 1 reverse transcriptase. *Antimicrob. Agents Chemother.*, **37**, 2231–2234.
45. Tisdale,M., Kemp,S.D., Parry,N.R. and Larder,B.A. (1993) Rapid in vitro selection of human immunodeficiency virus type 1 resistant to 3′-thiacytidine inhibitors due to a mutation in the YMDD region of reverse transcriptase. *Proc. Natl Acad. Sci. USA*, **90**, 5653–5656.
46. Menendez-Arias,L. (2010) Molecular basis of human immunodeficiency virus drug resistance: an update. *Antiviral Res.*, **85**, 210–231.
47. Sarafianos,S.G., Das,K., Hughes,S.H. and Arnold,E. (2004) Taking aim at a moving target: designing drugs to inhibit drug-resistant HIV-1 reverse transcriptases. *Curr. Opin. Struct. Biol.*, **14**, 716–730.
48. Menendez-Arias,L. (2010) Molecular basis of human immunodeficiency virus drug resistance: an update. *Antiviral Res.*, **85**, 210–231.
49. Menendez-Arias,L. and Berkhout,B. (2008) Retroviral reverse transcription. *Virus Res.*, **134**, 1–3.
50. Shi,Q., Singh,K., Srivastava,A., Kaushik,N. and Modak,M.J. (2002) Lysine 152 of MuLV reverse transcriptase is required for the integrity of the active site. *Biochemistry*, **41**, 14831–14842.
51. Johnson,K.A. (1993) Conformational coupling in DNA polymerase fidelity. *Annu. Rev. Biochem.*, **62**, 685–713.
52. Rezende,L.F. and Prasad,V.R. (2004) Nucleoside-analog resistance mutations in HIV-1 reverse transcriptase and their influence on polymerase fidelity and viral mutation rates. *Int. J. Biochem. Cell Biol.*, **36**, 1716–1734.
53. Paprotka,T., Venkatachari,N.J., Chaipan,C., Burdick,R., Delviks-Frankenberry,K.A., Hu,W.S. and Pathak,V.K. Inhibition of xenotropic murine leukemia virus-related virus by APOBEC3 proteins and antiviral drugs. *J. Virol.*, **84**, 5719–5729.
54. Sakuma,R., Sakuma,T., Ohmine,S., Silverman,R.H. and Ikeda,Y. (2010) Xenotropic murine leukemia virus-related virus is susceptible to AZT. *Virology*, **397**, 1–6.
55. Singh,I.R., Gorzynski,J.E., Drobysheva,D., Bassit,L. and Schinazi,R.F. (2010) Raltegravir is a potent inhibitor of XMRV, a virus implicated in prostate cancer and chronic fatigue syndrome. *PLoS One*, **5**, e9948.
56. Smith,R.A., Gottlieb,G.S. and Miller,A.D. (2010) Susceptibility of the human retrovirus XMRV to antiretroviral inhibitors. *Retrovirology*, **7**, 70.
57. Kawamoto,A., Kodama,E., Sarafianos,S.G., Sakagami,Y., Kohgo,S., Kitano,K., Ashida,N., Iwai,Y., Hayakawa,H., Nakata,H. *et al.* (2008) 2′-deoxy-4′-C-ethynyl-2-halo-adenosines active against drug-resistant human immunodeficiency virus type 1 variants. *Int. J. Biochem. Cell Biol.*, **40**, 2410–2420.
58. Kodama,E.I., Kohgo,S., Kitano,K., Machida,H., Gatanaga,H., Shigeta,S., Matsuoka,M., Ohrui,H. and Mitsuya,H. (2001) 4′-Ethynyl nucleoside analogs: potent inhibitors of multidrug-resistant human immunodeficiency virus variants in vitro. *Antimicrob. Agents Chemother.*, **45**, 1539–1546.
59. Kissel,J.D., Held,D.M., Hardy,R.W. and Burke,D.H. (2007) Single-stranded DNA aptamer RT1t49 inhibits RT polymerase and RNase H functions of HIV type 1, HIV type 2, and SIVCPZ RTs. *AIDS Res. Hum. Retroviruses.*, **23**, 699–708.
60. Chen,H. and Gold,L. (1994) Selection of high-affinity RNA ligands to reverse transcriptase: inhibition of cDNA synthesis and RNase H activity. *Biochemistry*, **33**, 8746–8756.
61. Joshi,P.J., Fisher,T.S. and Prasad,V.R. (2003) Anti-HIV inhibitors based on nucleic acids: emergence of aptamers as potent antivirals. *Curr. Drug Targets Infect. Disord.*, **3**, 383–400.
62. DeStefano,J.J. and Nair,G.R. (2008) Novel aptamer inhibitors of human immunodeficiency virus reverse transcriptase. *Oligonucleotides*, **18**, 133–144.
63. DeStefano,J.J. and Cristofaro,J.V. (2006) Selection of primer-template sequences that bind human immunodeficiency virus reverse transcriptase with high affinity. *Nucleic Acids Res.*, **34**, 130–139.
64. Arion,D., Kaushik,N., McCormick,S., Borkow,G. and Parniak,M.A. (1998) Phenotypic mechanism of HIV-1 resistance to 3′-azido-3′-deoxythymidine (AZT): increased polymerization processivity and enhanced sensitivity to pyrophosphate of the mutant viral reverse transcriptase. *Biochemistry*, **37**, 15908–15917.
65. Sarafianos,S.G., Hughes,S.H. and Arnold,E. (2004) Designing anti-AIDS drugs targeting the major mechanism of HIV-1 RT resistance to nucleoside analog drugs. *Int. J. Biochem. Cell Biol.*, **36**, 1706–1715.
66. Shafer,R.W., Kozal,M.J., Winters,M.A., Iversen,A.K., Katzenstein,D.A., Ragni,M.V., Meyer,W.A. 3rd, Gupta,P., Rasheed,S., Coombs,R. *et al.* (1994) Combination therapy with zidovudine and didanosine selects for drug-resistant human immunodeficiency virus type 1 strains with unique patterns of pol gene mutations. *J. Infect. Dis.*, **169**, 722–729.
67. Shirasaka,T., Kavlick,M.F., Ueno,T., Gao,W.Y., Kojima,E., Alcaide,M.L., Chokekijchai,S., Roy,B.M., Arnold,E., Yarchoan,R. *et al.* (1995) Emergence of human immunodeficiency virus type 1 variants with resistance to multiple dideoxynucleosides in patients receiving therapy with dideoxynucleosides. *Proc. Natl Acad. Sci. USA*, **92**, 2398–2402.
68. Iversen,A.K., Shafer,R.W., Wehrly,K., Winters,M.A., Mullins,J.I., Chesebro,B. and Merigan,T.C. (1996) Multidrug-resistant human immunodeficiency virus type 1 strains resulting from combination antiretroviral therapy. *J. Virol.*, **70**, 1086–1090.
69. Winters,M.A., Shafer,R.W., Jellinger,R.A., Mamtora,G., Gingeras,T. and Merigan,T.C. (1997) Human immunodeficiency virus type 1 reverse transcriptase genotype and drug susceptibility changes in infected individuals receiving dideoxyinosine monotherapy for 1 to 2 years. *Antimicrob. Agents Chemother.*, **41**, 757–762.
70. Gu,Z., Gao,Q., Fang,H., Salomon,H., Parniak,M.A., Goldberg,E., Cameron,J. and Wainberg,M.A. (1994) Identification of a mutation at codon 65 in the IKKK motif of reverse transcriptase that encodes human immunodeficiency virus resistance to 2′,3′-dideoxycytidine and 2′,3′-dideoxy-3′-thiacytidine. *Antimicrob. Agents Chemother.*, **38**, 275–281.
71. Knox,K., Carrigan,D., Simmons,G., Teque,F., Zhou,Y., Hackett,J. Jr., Qiu,X., Luk,K.C., Schochetman,G., Knox,A. *et al.* (2011) No evidence of murine-like gammaretroviruses in CFS patients previously identified as XMRV-infected. *Science*.
72. Oakes,B., Tai,A.K., Cingoz,O., Henefield,M.H., Levine,S., Coffin,J.M. and Huber,B.T. (2010) Contamination of human DNA samples with mouse DNA can lead to false detection of XMRV-like sequences. *Retrovirology*, **7**, 109.
73. Robinson,M.J., Erlwein,O.W., Kaye,S., Weber,J., Cingoz,O., Patel,A., Walker,M.M., Kim,W.J., Uiprasertkul,M., Coffin,J.M.

et al. (2010) Mouse DNA contamination in human tissue tested for XMRV. *Retrovirology*, **7**, 108.
74. Sato,E., Furuta,R.A. and Miyazawa,T. (2010) An endogenous murine leukemia viral genome contaminant in a commercial RT-PCR kit is amplified using standard primers for XMRV. *Retrovirology*, **7**, 110.
75. Coffin,J.M. and Stoye,J.P. (2009) Virology. A new virus for old diseases? *Science*, **326**, 530–531.
76. Huang,H., Chopra,R., Verdine,G.L. and Harrison,S.C. (1998) Structure of a covalently trapped catalytic complex of HIV-1 reverse transcriptase: implications for drug resistance. *Science*, **282**, 1669–1675.
77. Sarafianos,S.G., Das,K., Tantillo,C., Clark,A.D. Jr., Ding,J., Whitcomb,J.M., Boyer,P.L., Hughes,S.H. and Arnold,E. (2001) Crystal structure of HIV-1 reverse transcriptase in complex with a polypurine tract RNA:DNA. *EMBO J.*, **20**, 1449–1461.
78. Kirby,K.A., Singh,K., Michailidis,E., Marchand,B., Kodama,E.N., Ashida,N., Mitsuya,H., Parniak,M.A. and Sarafianos,S.G. The sugar ring conformation of 4′-ethynyl-2-fluoro-2′-deoxyadenosine and its recognition by the polymerase active site of hiv reverse transcriptase. *Cell Mol. Biol.*, **57**, 40–46.
79. Gotte,M., Arion,D., Parniak,M.A. and Wainberg,M.A. (2000) The M184V mutation in the reverse transcriptase of human immunodeficiency virus type 1 impairs rescue of chain-terminated DNA synthesis. *J. Virol.*, **74**, 3579–3585.
80. Wainberg,M.A., Drosopoulos,W.C., Salomon,H., Hsu,M., Borkow,G., Parniak,M., Gu,Z., Song,Q., Manne,J., Islam,S. *et al.* (1996) Enhanced fidelity of 3TC-selected mutant HIV-1 reverse transcriptase. *Science*, **271**, 1282–1285.
81. Pandey,V.N., Kaushik,N., Rege,N., Sarafianos,S.G., Yadav,P.N. and Modak,M.J. (1996) Role of methionine 184 of human immunodeficiency virus type-1 reverse transcriptase in the polymerase function and fidelity of DNA synthesis. *Biochemistry*, **35**, 2168–2179.
82. Das,K., Bandwar,R.P., White,K.L., Feng,J.Y., Sarafianos,S.G., Tuske,S., Tu,X., Clark,A.D. Jr., Boyer,P.L., Hou,X. *et al.* (2009) Structural basis for the role of the K65R mutation in HIV-1 reverse transcriptase polymerization, excision antagonism, and tenofovir resistance. *J. Biol. Chem.*, **284**, 35092–35100.
83. Meyer,P.R., Matsuura,S.E., Mian,A.M., So,A.G. and Scott,W.A. (1999) A mechanism of AZT resistance: an increase in nucleotide-dependent primer unblocking by mutant HIV-1 reverse transcriptase. *Mol. Cell.*, **4**, 35–43.
84. Ueno,T., Shirasaka,T. and Mitsuya,H. (1995) Enzymatic characterization of human immunodeficiency virus type 1 reverse transcriptase resistant to multiple 2′,3′-dideoxynucleoside 5′-triphosphates. *J. Biol. Chem.*, **270**, 23605–23611.
85. Rhee,S.Y., Gonzales,M.J., Kantor,R., Betts,B.J., Ravela,J. and Shafer,R.W. (2003) Human immunodeficiency virus reverse transcriptase and protease sequence database. *Nucleic Acids Res.*, **31**, 298–303.

Published in final edited form as:
Cell Mol Biol (Noisy-le-grand). ; 58(1): 187–195.

EFFECT OF TRANSLOCATION DEFECTIVE REVERSE TRANSCRIPTASE INHIBITORS ON THE ACTIVITY OF N348I, A CONNECTION SUBDOMAIN DRUG RESISTANT HIV-1 REVERSE TRANSCRIPTASE MUTANT

E. MICHAILIDIS[1], **K. SINGH**[1], **E.M. RYAN**[1], **A. HACHIYA**[1], **Y.T. ONG**[1], **K.A. KIRBY**[1], **B. MARCHAND**[1], **E.N. KODAMA**[2], **H. MITSUYA**[3], **M.A. PARNIAK**[4], and **S.G. SARAFIANOS**[1,5,*]

[1]Christopher S. Bond Life Sciences Center and Department of Molecular Microbiology & Immunology, School of Medicine, University of Missouri, Columbia, MO 65211, USA

[2]Division of Emerging Infectious Diseases, Tohoku University School of Medicine, Sendai 980-8575, Japan

[3]Department of Hematology and Infectious Diseases, Kumamoto University, Kumamoto 860-8556, Japan & Experimental Retrovirology Section, HIV/AIDS Malignancy Branch, NIH, Bethesda, MD 20892, USA

[4]Department of Molecular Genetics & Biochemistry University of Pittsburgh School of Medicine, Pittsburgh, PA 15261, USA

[5]Department of Biochemistry, University of Missouri, Columbia, MO 65211, USA

Abstract

4′-ethynyl-2-fluoro-2′-deoxyadenosine (EFdA) is a highly potent inhibitor of HIV-1 reverse transcriptase (RT). We have previously shown that its exceptional antiviral activity stems from a unique mechanism of action that is based primarily on blocking translocation of RT; therefore we named EFdA a Translocation Defective RT Inhibitor (TDRTI). The N348I mutation at the connection subdomain (CS) of HIV-1 RT confers clinically significant resistance to both nucleoside (NRTIs) and non-nucleoside RT inhibitors (NNRTIs). In this study we tested EFdA-triphosphate (TP) together with a related compound, ENdA-TP (4′-ethynyl-2-amino-2′-deoxyadenosine triphosphate) against HIV-1 RTs that carry clinically relevant drug resistance mutations: N348I, D67N/K70R/L210Q/T215F, D67N/K70R/L210Q/T215F/N348I, and A62V/V75I/F77L/F116Y/Q151M. We demonstrate that these enzymes remain susceptible to TDRTIs. Similar to WT RT, the N348I RT is inhibited by EFdA mainly at the point of incorporation through decreased translocation. In addition, the N348I substitution decreases the RNase H cleavage of DNA terminated with EFdA-MP ($T/P_{EFdA\text{-}MP}$). Moreover, N348I RT unblocks EFdA-terminated primers with similar efficiency as the WT enzyme, and further enhances EFdA unblocking in the background of AZT-resistance mutations. This study provides biochemical insights into the mechanism of inhibition of N348I RT by TDRTIs and highlights the excellent efficacy of this class of inhibitors against WT and drug-resistant HIV-1 RTs.

Keywords

EFdA; ENdA; N348I; Translocation Defective Reverse Transcriptase Inhibitors; Reverse Transcriptase; HIV-1; Antivirals

*Correspond to: sarafianoss@missouri.edu, Phone: 573-882-4338, Fax: 573-884-9676.